RSC Applied Interfaces



REVIEW

View Article Online



Cite this: RSC Appl. Interfaces, 2024,

Recent advances in semiconductor heterojunctions: a detailed review of the fundamentals of photocatalysis, charge transfer mechanism and materials

Aniket Balapure, Pa Javati Ray Dutta ** and Ramakrishnan Ganesan ** and Ramakrishnan Ganesan **.

Photocatalysis, due to its operability under sustainable and green energy conditions, is one of the cardinal branches of the environmental remediation domain. To date, a significant amount of work has been carried out in the design and development of various photocatalysts for applications such as dye degradation, CO₂ and NO_v reduction, organic transformation and hydrogen generation. Among several factors leading to enhancement of the photocatalytic activity, decreasing the electron-hole (exciton) recombination is regarded as one of the prime factors. Typically, the lifetime of the excitons can be increased by combining two or more semiconductors via forming a heterojunction. Various types of heterojunctions, such as the Schottky barrier, p-n (or non-p-n), van der Waals and facet heterojunctions, can be fabricated depending on specific applications. Each type of heterojunction has its advantages and limitations; hence, proper choice of heterojunction is essential. Almost all classes of semiconductor materials, for instance, metal oxide, perovskites, chalcogenides, metal-organic frameworks (MOFs), covalent organic frameworks (COFs) and MXenes, with a suitable band gap, have been studied for photocatalysis. This review details different classes of materials and types of heterojunctions from the recent literature to provide the reader with a deeper understanding of the same. Initially, the fundamentals of photocatalysis and its basic mechanism are discussed, followed by a detailed discussion on the various types of heterojunctions based on the charge transfer mechanism, such as types I, II and III, with representative examples from recent reports. This panoramic review attempts to encourage a rational design of heterojunctions by choosing the proper candidates to push the process efficiency to its limit.

Received 5th August 2023, Accepted 26th September 2023

DOI: 10.1039/d3lf00126a

rsc.li/RSCApplInter

Introduction

The expanding population and industrial establishments, which have paved the way for rapid developments and, consequently, increased the energy requirements, have contributed to the obliterating level of air, water and soil pollution. These factors have led to an increased awareness and, thereby, further exploration of possible approaches toward environmental remediation. 1-3

Photocatalysis—a process that employs the combination of a semiconductor and an appropriate light source-has recently emerged as one of the promising technologies contributing to the generation of renewable energy sources, as well as water decontamination.4,5 In 1969, Muller discovered the photocatalytic degradation of isopropanol by ZnO.6 Following that, in 1972, researchers K. Honda and A. Fujishima discovered the water-splitting mechanism by employing TiO2.7 Since then TiO2 has remained a popular choice of photocatalyst in several domains, owing to its beneficial characteristics, such as chemical stability, non-toxicity and high reactivity.^{8,9} Due to the wide band gap in these materials, in the past, photocatalysis was mainly performed using ultraviolet radiation-based processes. Recently, there has been a surge of interest in utilizing solar energy for these purposes due to its abundant availability. It has been estimated that the amount of solar energy striking the Earth's surface in an hour is much higher than the global annual energy consumption. While the world's primary energy demand is expected to grow to the tune of 30% by 2040, the share of renewable energy does not exceed 40% by 2040.¹⁰ These facts highlight the necessity to substantiate the

^a Department of Chemistry, Birla Institute of Technology and Science (BITS), Pilani, Hyderabad Campus, Jawahar Nagar, Kapra Mandal, Medchal District, Hyderabad, Telangana, 500078, India. E-mail: ram.ganesan@hyderabad.bits-pilani.ac.in ^b Department of Biological Sciences, Birla Institute of Technology and Science (BITS), Pilani, Hyderabad Campus, Iawahar Nagar, Kapra Mandal, Medchal District, Hyderahad, Telangana, 500078, India. E-mail: jayati@hyderabad.bits-pilani.ac.in

research efforts to increase the share of renewable energy for future needs.

In a typical photocatalytic process, the movement of electrons from the valence band (VB) to the conduction band (CB) occurs, creating a hole in the VB. This phenomenon is triggered by the irradiation of a photon with an energy equal to or greater than the band gap of the semiconductor. Such photogenerated electrons and holes are the active species that are primarily responsible for various photocatalytic activities. Most of the photogenerated electrons and holes recombine, a process that is detrimental to photocatalytic performance. The minimization of the electron-hole (exciton) recombination, as indicated by its increased lifetime, was realized as an efficient strategy to enhance the overall process efficiency. Since the discovery of interparticle electron transfer by Serpone et al. in 1984, combining two semiconductors to avert the charge combination has become a popular strategy.¹¹ A decade later, the interparticle hole transfer was also affirmed, and since then, combining the two semiconductors for heterojunction formation has been a monstrously investigated zone in photocatalysis.¹²

As opposed to the conventional catalytic process, semiconductor catalysis relies mainly on the excitons for the various redox reactions. 13-16 The major drawback in singlecomponent catalysts is the high recombination rate, resulting in poor photocatalytic activity. The recombination rate can be addressed by the formation of a heterojunction, which is one of the driving forces for the extensive ongoing work in the development of heterojunction catalysts. Additionally, it can offer greater selectivity due to the specific redox potential of the excitons due to their various types of heterojunctions.

The number of publications regarding heterojunction in photocatalysis published between the years 1999 and 2022 is shown in the graph (Fig. 1(a)). In photocatalysis, certain discoveries have been proven to be pivotal for the development of the domain, as shown in Fig. 1(b).

This panoramic review gives a nitty-gritty discourse on the various perspectives of heterojunction photocatalysis. It covers the fundamental principles of photocatalysis and presents a detailed discussion on various types of heterojunctions based on the electron-hole hopping pathway, such as type I, type II, type III, type B, Z-scheme, and S-scheme. Various heterojunctions from recent reports, such as the Schottky barrier, p-n, and non-p-n semiconductor, van der Waals, organic, and facet heterojunctions, are also discussed.

All sorts of semiconducting materials, such as MXenes, metal-organic frameworks (MOFs), covalent organic frameworks (COFs), metal oxides, perovskites, etc., with appropriate band gaps, are deployed for the heterojunction fabrication, and hence representative reports are discussed under the 'Library of materials used for heterojunction formation in photocatalysis' section.

A list of the selected recent heterojunction photocatalysts is represented in the tables based on the type of the heterojunction fabricated, such as type I, type II, Z-scheme, and S-scheme. Various parameters like synthetic protocol, reaction rate, experimental conditions, light source, etc., are given and future perspectives are discussed.

Fundamentals in photocatalysis

Before going further, the reader is encouraged to consult the review by Schneider et al. on the mechanisms of TiO2 photocatalysis, which discusses the processes under dark and light conditions, causing band bending and flattening. 8 Band bending was first discussed by Schottky and Mott and occurs at the metal-semiconductor junction. The energy band edges in the semiconductor are shifted due to the charge transfer at the metal-semiconductor junction and this is termed band bending. The upward bend is observed when the work function of the metal is greater than that of the semiconductor. However, when the semiconductor work function is greater than the metal work function, downward band bending is observed. Apart from this, band bending of the band edges of the semiconductor can be observed due to an applied external field, adsorption on the semiconductor surface and surface states. The flat energy band (zero space

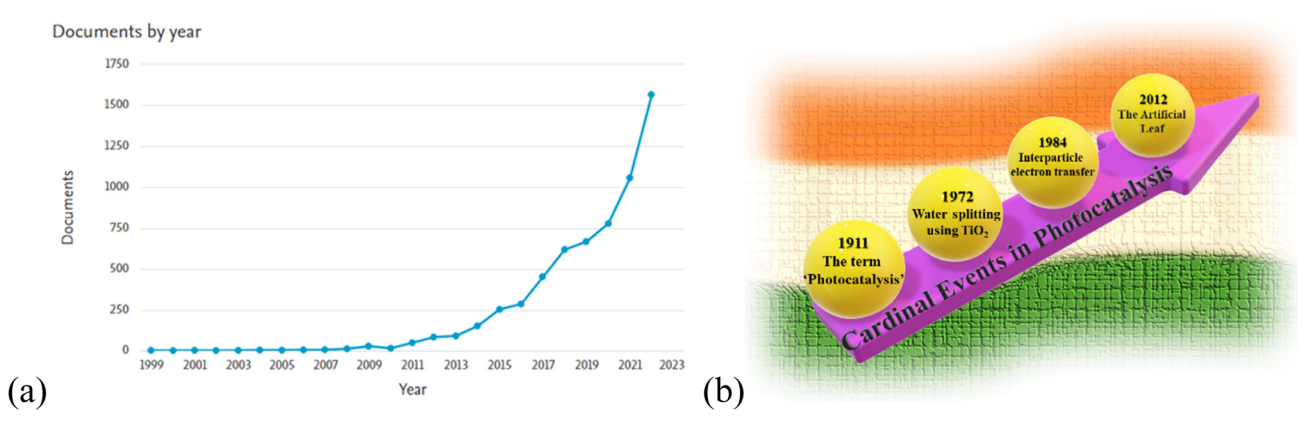


Fig. 1 (a) The trend in the number of publications obtained from 'Scopus' with the keyword 'heterojunction photocatalysis' accessed on January 3, 2023. (b) Important milestones in the field of photocatalysis.

charge in the semiconductor) is observed when there is zero bias voltage between the metal and the semiconductor. 17

A typical photocatalytic mineralization process involves several steps, including the generation of excitons, their separation, and the production of reactive oxygen species (ROS). The salient mechanistic steps in the photodegradation of an organic pollutant are listed below.

Photoexcitation: Photocatalyst +
$$hv \rightarrow e_{CB}^- + h_{VB}^+$$
 (1)

Electron-hole recombination:
$$e_{CB}^- + h_{VB}^+ \rightarrow heat/light$$
 (2)

Formation of hydroxyl radical:
$${}^{-}OH + h_{VB}^{^{}} \rightarrow {}^{\cdot}OH$$
 (3)

Formation of superoxide anion radical:
$$(O_2)_{Ads} + e_{CB} \rightarrow O_2$$
 (4)

Formation of hydrogen peroxide:
$$^{-}O_2$$
 + $H^+ \rightarrow ^{+}O_2H$ (5)

$${}^{\bullet}O_{2}H + e_{CB}^{} \rightarrow HO_{2}^{}$$
 (6)

$$HO_2^- + H^+ \to H_2O_2$$
 (7)

Organic pollutant +
$$h^+ \rightarrow Fragments/CO_2 + H_2O$$
 (9)

Depending on the duration of illumination, either fragments or complete mineralization of the organic pollutants can be achieved. 18-24 For further details on ROS generation mechanisms and detection methods, the reader is encouraged to review the comprehensive survey by Nosaka et al.²⁵

What is a heterojunction?

As mentioned earlier, to enhance the lifetime of excitons, two different semiconductors, or a semiconductor and a metal, or a semiconductor and a carbonaceous compound, are coupled decrease electron-hole recombination. Such combination of materials with dissimilar band diagrams results in a new electronic structure after hybridization. The band bending is created at the interface of the two semiconductors/components, resulting in potential difference between the two semiconductor regions. The interface, therefore, induces an electric field within the space charge region that is useful for the spatial separation of the photogenerated excitons, which is termed a 'heterojunction'.26

Due to the low dielectric constant in organic semiconductors, charge separation is inefficient. It results in coulombically bound excitons as opposed to inorganic semiconductors. Hence, various heterojunctions have been prepared for organic semiconductors to enhance the charge separation efficacy. Moreover, heterojunctions are fabricated

for inorganic semiconductors as well to improve the charge separation efficiency and light absorption characteristics.²⁷

Factors affecting heterojunctions

The efficacy of the heterojunction is controlled by several factors. The intimate contact between the components is the primary condition for effective charge separation and the formation of an inbuilt electric field at the interface. The positions of the CB and VB play a critical role in the effective transfer of the electrons and holes and depend on the type of heterojunction achieved. The built-in electric field and potential barriers at the heterojunction interface also depend on other factors such as semiconductivity (n type or p type), work function, and Fermi level.²⁸

Besides the above factors, one may need to consider the orientation between the two components forming the heterojunction. For instance, Xiong et al. fabricated three heterojunction interfaces consisting of α-Fe₂O₃/Bi₂O₃ in "ring-to-face", "face-to-face", and "rod-to-face" orientations. It was found that the face-to-face model showed the highest photocatalytic activity owing to sufficient interfacial contact and adequate channels for efficient charge transfer.²⁹

Types of heterojunctions based on structural or compositional aspects

Depending on the structural or compositional aspects, photocatalysts can be classified into Schottky barrier, p-n (or non-p-n), van der Waals, and facet heterojunctions, which are briefly discussed below (Fig. 2).

Schottky barrier heterojunctions

Depending on the work function between two components, either an Ohmic contact or a Schottky barrier is generated at the interface between a semiconductor and a conductor. An Ohmic junction is formed when the work function of the semiconductor is higher than the conducting component. Ohmic contact facilitates the flow of electrons between the metal and semiconductor materials in both forward and reverse-biased directions. This results in poor charge separation and photoresponse. When the work function of semiconductor is smaller than the conducting component, it forms the Schottky barrier. The Schottky barrier facilitates the unilateral flow of electrons in the forward-biased direction, resulting in efficient charge separation.30

The facet engineering at the interface of TiO2 and Au and its impact on the Schottky contact barrier height have been explored by Wang et al. The lowering of the Schottky barrier in Au/TiO₂ (101), as compared to Au/TiO₂ (001), was found to facilitate the transfer of a photogenerated electron from the CB of TiO₂ to Au while encouraging the hot electron injections in the reverse direction. Such a process was reported to improve the photocatalytic activity of Au/TiO2 (101) toward the generation of CO and CH₄.³³ Pd nanocubes

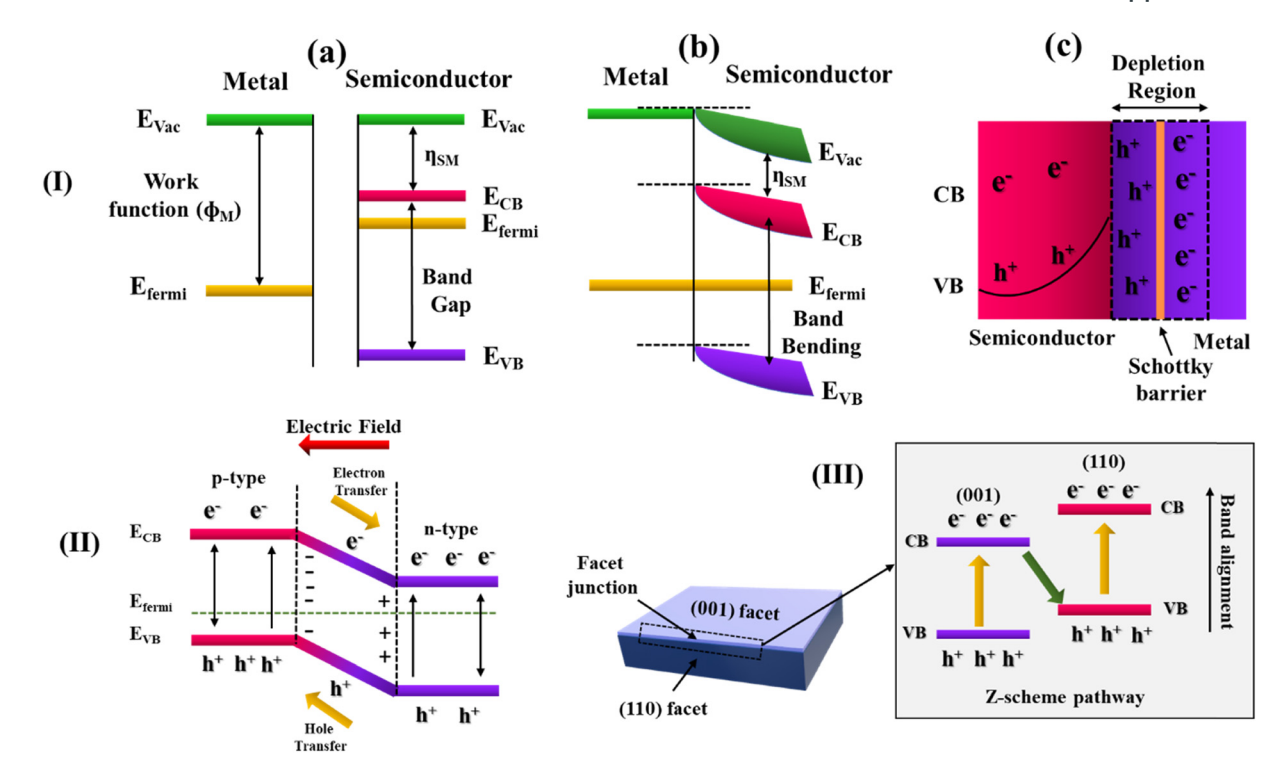


Fig. 2 Schematic diagram depicting the band structure along with the charge recombination processes in the (I) Schottky barrier, (II) p-n heterojunction and (III) facet junction. In (I), panels (a)-(c) represent the steps before contact, after contact and the creation of a Schottky-like barrier, respectively. The diagrams and notations in (I)-(III) were re-drawn/reproduced from ref. 30-32, respectively.

with {100} exposed facets and Pd nano-octahedrons with {111} exposed facets have been anchored on two-dimensional TiO₂ nanosheets by Lu et al. Pd with exposed facet {111} has demonstrated a greater rate of photocatalytic hydrogenation of nitroarenes. Their investigation revealed that Pd with the {111} exposed facet has a higher Schottky barrier as opposed to Pd with the {100} facet exposed. The higher Schottky barrier results in efficient interfacial charge separation and lower recombination of the photoexcited charge pairs.³⁴ Li et al. synthesized a MXene-based ternary system, CdS@Au/ Ti_{3-x}C₂T_v, which was found to possess a high hydrogen production rate of 5371 µmol g⁻¹ h⁻¹ under visible light irradiation. The enhancement in the activity was attributed to the 'dual Schottky barrier' formed at the interface of the ternary system.³⁵

p-n and non-p-n semiconductor heterojunctions

Depending on the type of semiconductors employed, there are two different forms of semiconductor-semiconductor heterojunction. The term 'p-n heterojunction' refers to the contact formed by p and n-type semiconductors. A 'non-p-n junction' is one in which there are two semiconductors, either n- or p-type, often possessing staggered band positions. For charge separation and collection, the p-n junction is an efficient architecture. At the interface, due to the diffusion of the holes and electrons, the p-n junction forms a space charge region, which creates an in-built electrical potential that directs the electrons and holes to travel in opposite directions.³¹

Metal-organic framework (MOF)-derived indium oxide/ bismuth oxyiodide was employed by Sun et al. to create a p-n junction photocatalyst. The as-synthesized photocatalyst has shown robust activity against phenolic pollutants, which is attributed to the interfacial charge transfer and increased quantum efficiency at the p-n junction.21 Liang et al. reported the enhancement in the TiO2/NiO p-n junction efficiency by incorporating a Pt co-catalyst that resulted in higher photocatalytic hydrogen evolution activity and stability. 36 Li et al. synthesized an NH2-UiO-66/CoFe2O4/ CdIn₂S₄ composite material to construct a double p-n junction exhibiting dual-carrier transfer channels, which was found to have a higher efficiency towards photocatalytic hydrogen evolution.37 Tian et al. fabricated a facet-chargeinduced coupling-dependent BiOI/g-C₃N₄ p-n junction, in which the catalyst with the {001} BiOI exposed facet was found to have a much higher photocatalytic activity towards industrial pollutants and antibiotic degradation than the catalyst having BiOI with the {110} facet.38

In the non-p-n junction, two semiconductors are generally coupled with the staggering band gap, which can be a type II heterojunction (vide infra).

van der Waals heterojunctions

After the discovery of graphene by Novoselov et al. in 2004, heterojunctions based on 2D sheet stacks of two different

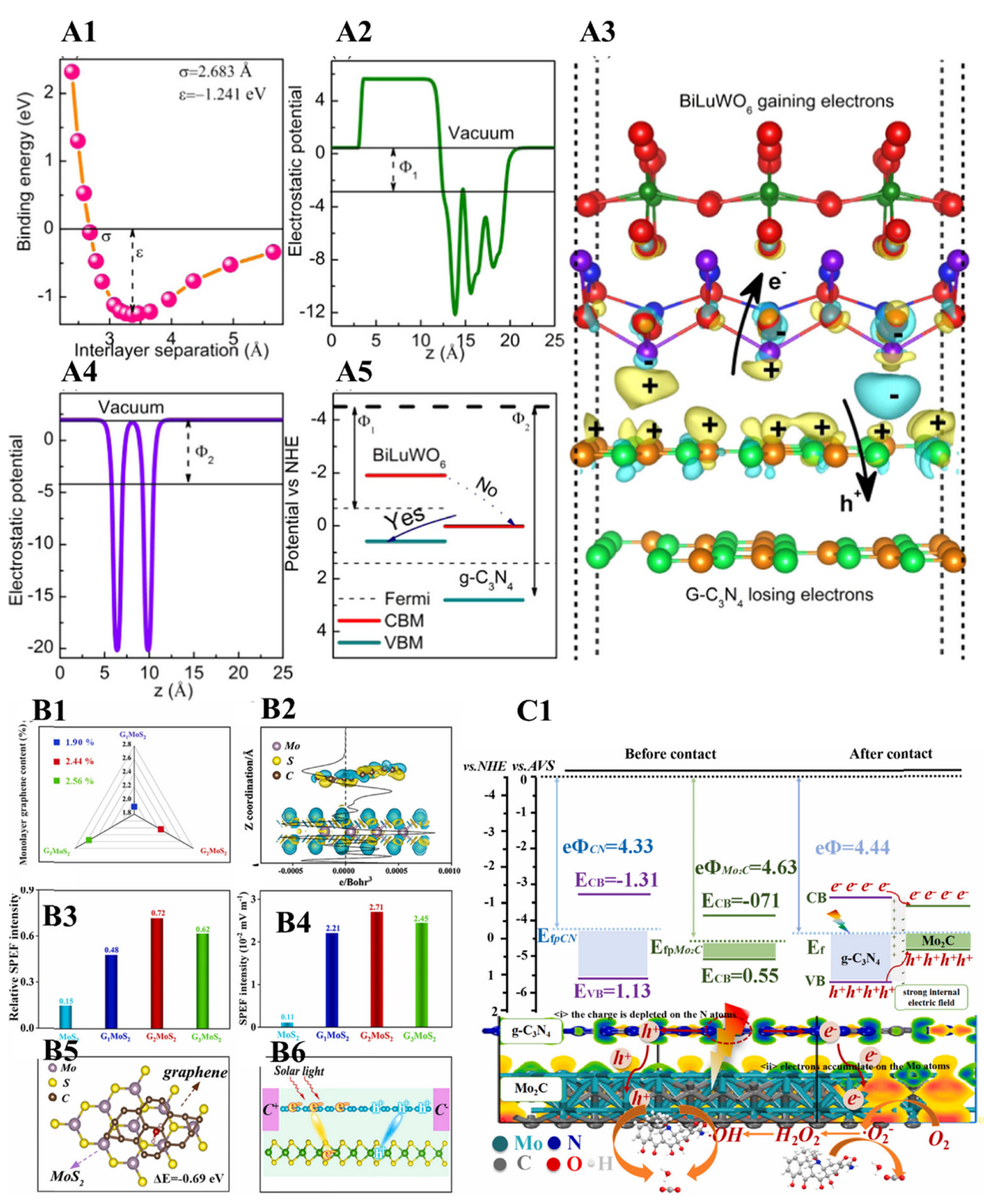


Fig. 3 Binding energies (A1), electrostatic potentials (A2 and A4) of BiLuWO₆ and g-C₃N₄, resulting Z-scheme (A5), charge density difference (with an isosurface value of 0.005 e bohr⁻³) and flow of excitons in the van der Waals heterojunction (A3). Reproduced with permission from ref. 41. Copyright 2021 American Chemical Society. Graphene contents (B1), differential and planar-average charge density (B2), relative SPEF intensity (B3), SPEF intensity (B4). H₂O molecule adsorption on GmoS₂ (top view, B5), migration and separation of excitons on GmoS₂ (B6). Reproduced with permission from ref. 43. Copyright 2022 Elsevier B.V. 2D Mo₂C/2Dg-C₃N₄ photocatalytic mechanism and charge transfer (C1). Reproduced with permission from ref. 42. Copyright 2021 Elsevier B.V.

Review

materials or multiple materials held by van der Waals forces were developed to enhance the performance of the individual components. 39,40 Jia et al. synthesized the g-C₃N₄/BiLuWO₆ heterojunction and investigated it in detail using theoretical studies.41 The theoretical and experimental studies confirmed the van der Waals heterojunction between the g-C₃N₄ and BiLuWO₆. A Z-scheme served as the charge transfer mechanism (vide infra). The photodegradation of Rhodamine B and methylene blue was faster by the g-C₃N₄/BiLuWO₆ van der Waals heterojunction than the individual phases (Fig. 3(A1-A5)).

Zhou et al. fabricated a 2D Mo₂C/2Dg-C₃N₄ van der Waals heterojunction (see Fig. 3(C1)),42 which facilitated the interlayer electron transfer, building an internal electric field stimulating the photogenerated charge kinetics. The assynthesized catalyst showed better activity for degrading waste pharmaceuticals and personal care products. Yao et al. fabricated a spin-polarized graphene monolayer-based van der Waals heterojunction on two-dimensional MoS2 (see 3(B1-B6)).⁴³ The theoretical and experimental investigation confirmed that the photogenerated electrons and holes were separated and directionally transferred from MoS₂ to the opposite regions of the monolayer graphene to form an 'electric field' via the van der Waals heterojunction. The as-synthesized heterojunction showed better results for

overall water splitting. Xu et al. developed a simple protocol for fabricating Bi₃O₄Cl/g-C₃N₄ van der Waals heterostructures for effective CO₂ photoreduction. 44 A review article devoted to the theoretical studies on 2D van der Waals heterostructures for functional material and devices was reported by Hu et al. 45

Facet heterojunction

Heterojunctions are also created within the same material but between two different facets. A study by Zhao et al. reported a decrease in charge recombination by forming a heterojunction between the {110} and {001} facets of BiOCl nanoplates.32 It was found that the facet ratio was crucial in determining photocatalytic activity.

By anchoring AgBr-Ag nanoparticles to the exposed {010} facets of BiVO₄ microplates (Fig. 4(A1-A12)), a facet heterojunction was prepared, which showed an improved photocatalytic bacterial inactivation.⁴⁶

Luo al. fabricated etfacet heterojunction CdS-Au- $\{010\}$ BiVO₄ $\{110\}$ -MnO_x, for photothermocatalyst, toluene degradation (see Fig. 4(B1-B10)).47 This was obtained by the selective deposition of CdS-Au and MnOx over the {010} and {110} facets of BiVO₄ crystals, respectively. An

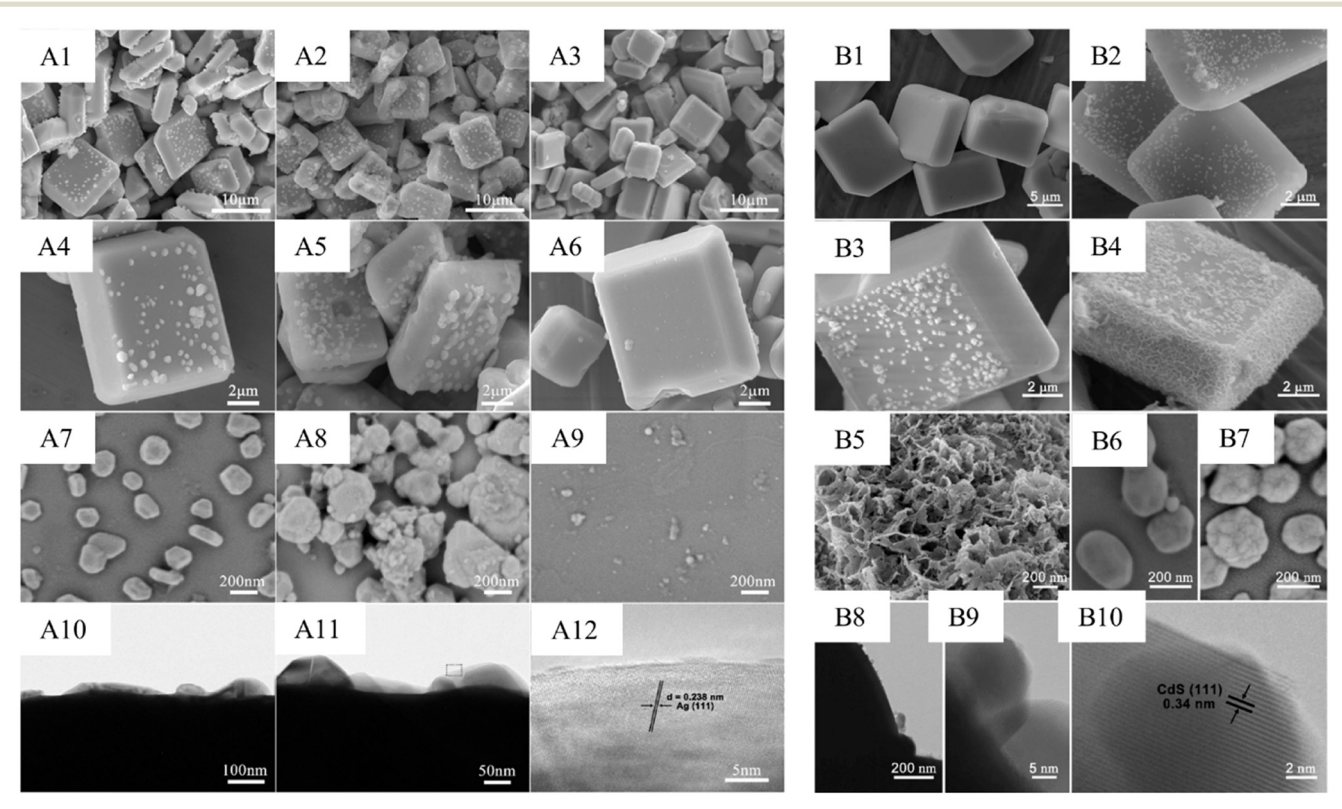


Fig. 4 SEM images of Ag-BiVO₄{010} (A1 and A4), AgBr-Ag-BiVO₄{010} (A2 and A5), and Ag-BiVO₄{010} (Na₂S₂O₃ treated) (A3 and A6). FE-SEM images of Ag-BiVO₄(010) (A7), AgBr-Ag-BiVO₄(010) (A8), and Ag-BiVO₄(010) (Na₂S₂O₃ treated) (A9). HR-TEM images of AgBr-Ag-BiVO₄ (A10-A12). Reproduced with permission from ref. 46. Copyright 2020 American Chemical Society. SEM images of BiVO₄ (B1), Au-{010}BiVO₄ (B2), CdS-Au- $\{010\}$ BiVO₄ (B3), CdS-Au- $\{010\}$ BiVO₄ $\{110\}$ -MnO_x (B4), FE-SEM images of MnO_x on $\{110\}$ facet of CdS-Au- $\{010\}$ BiVO₄ $\{110\}$ -MnO_x (B5), FE-SEM images of MnO_x on $\{110\}$ facet of CdS-Au- $\{010\}$ BiVO₄ $\{110\}$ -MnO_x (B5), FE-SEM images of MnO_x on $\{110\}$ facet of CdS-Au- $\{010\}$ BiVO₄ $\{110\}$ -MnO_x (B5), FE-SEM images of MnO_x on $\{110\}$ facet of CdS-Au- $\{010\}$ BiVO₄ $\{110\}$ -MnO_x (B5), FE-SEM images of MnO_x on $\{110\}$ facet of CdS-Au- $\{010\}$ BiVO₄ $\{110\}$ -MnO_x (B5), FE-SEM images of MnO_x on $\{110\}$ facet of CdS-Au- $\{010\}$ BiVO₄ $\{110\}$ -MnO_x (B5), FE-SEM images of MnO_x on $\{110\}$ facet of CdS-Au- $\{010\}$ BiVO₄ $\{110\}$ -MnO_x (B5), FE-SEM images of MnO_x on $\{110\}$ facet of CdS-Au- $\{010\}$ BiVO₄ $\{110\}$ -MnO_x (B5), FE-SEM images of MnO_x on $\{110\}$ facet of CdS-Au- $\{010\}$ BiVO₄ $\{110\}$ -MnO_x (B5), FE-SEM images of MnO_x on $\{110\}$ facet of CdS-Au- $\{010\}$ BiVO₄ $\{110\}$ -MnO_x (B5), FE-SEM images of MnO_x on $\{110\}$ facet of CdS-Au- $\{010\}$ BiVO₄ $\{110\}$ -MnO_x (B5), FE-SEM images of MnO_x on $\{110\}$ facet of CdS-Au- $\{010\}$ BiVO₄ $\{110\}$ -MnO_x (B5), FE-SEM images of MnO_x on $\{110\}$ facet of CdS-Au- $\{010\}$ BiVO₄ $\{110\}$ -MnO_x (B5), FE-SEM images of MnO_x on $\{110\}$ facet of CdS-Au- $\{010\}$ BiVO₄ $\{110\}$ -MnO_x (B5), FE-SEM images of MnO_x on $\{110\}$ facet of CdS-Au- $\{010\}$ BiVO₄ $\{110\}$ -MnO_x (B5), FE-SEM images of MnO_x on $\{110\}$ facet of CdS-Au- $\{010\}$ BiVO₄ $\{110\}$ -MnO_x (B5), FE-SEM images of MnO_x on $\{110\}$ facet of CdS-Au- $\{010\}$ BiVO₄ $\{110\}$ -MnO_x (B5), FE-SEM images of MnO_x on $\{110\}$ images of Au NPs on {010} facet of Au-{010}BiVO₄ (B6). FE-SEM images of CdS-Au NPs on {010} facet of CdS-Au-{010}BiVO₄{110}-MnO_x (B7). HR-TEM images of CdS-Au-{010}BiVO₄{110}-MnO_x (B8-B10). Reproduced with permission from ref. 47. Copyright 2022 Elsevier B.V.

adjustable {312}/{004} facet heterojunction was created by Gao et al. using multi-walled carbon nanotubes (MWCNTs) and Bi₅O₇I.⁴⁸ Ofloxacin, a typical antibiotic, was degraded well when exposed to light due to the enhancement of charge separation by the S-scheme (vide infra). Zhang et al. deployed the directional loading of Cu₂O on the [100] facet of BiOCl to create the facet heterojunction.⁴⁹ Upon irradiation, electrons generated in Cu₂O were transmitted to the [100] facet of BiOCl through the Z-scheme to result in the highly efficient photocatalytic synthesis of ammonia.

Types of heterojunctions based on the charge separation mechanism

Heterojunctions are also classified based on the band positions and charge transfer mechanism, which are discussed in this section.

Based on the position of the CB and VB, there are three major types of heterojunctions: type I (straddling gap), type II (staggering gap), and type III (broken gap), as shown in Fig. 5.

Type I

In the type I heterojunction, a semiconductor component having a smaller bandgap is interfaced with a second semiconductor such that the CB and VB levels of the former lie between those of the latter, thus resulting in a straddling band alignment. Upon light irradiation with suitable energy, the photogenerated charge carriers of the second component (higher bandgap) hop to the first component (lower bandgap). This phenomenon causes charge accumulation in the component with the lower bandgap. It is generally regarded that the charge separation efficiency is relatively low in type I heterojunctions since all the charge accumulation occurs in one of the components. 26,50 Nevertheless, the right choice of materials has shown better

behaviour in the type I heterojunction systems when compared to the individual components. Zhao et al. fabricated ZnS@ZnIn2S4 core-shell cages with the type I heterojunction configuration, which resulted in the high absorption of the incident photons and effective separation of the photogenerated excitons, and thereby higher CO₂ photoreduction activity.⁵¹ Another study reported a similar configuration in the CuO/BaTiO3 system, wherein the built-in potential at the nanointerface showed enhanced activity for methyl orange degradation and CO2 sensing properties. The enhancement was attributed to the compatible type I p/n heterojunction.⁵² Challagulla et al. reported a system comprised of a TiO2 shell supported over a Fe3O4 core, in which Fe₂O₃ formation was observed at the interface during the synthesis. While the Fe₃O₄ core facilitated the magnetic recovery and reusability of the photocatalyst, the type I heterojunction formed between TiO2 and Fe2O3 enhanced the photocatalytic Cr(v1) reduction under an aerobic atmosphere as compared to the individual components.⁵³

Type II

The type II heterojunction is considered more effective than the type I counterpart. Due to the staggering band edge potentials, the charge carriers flow in opposite directions, resulting in effective charge separation. Consequently, many type II heterojunctions are reported in the literature due to the higher charge separation efficiency, resulting in improved photocatalytic activity.26,50 Zhang et al. prepared a type II heterojunction consisting of tin sulphide and the indium(III) sulphide, SnS₂/In₂S₃, by deploying a one-pot hydrothermal synthesis method.54 This type II heterojunction between SnS2 and In₂S₃ resulted in the effective separation of the excitons, with 99.2 and 15.3 times higher photodegradation activity in Rhodamine B than the respective individual components. The same study reported the enhancement in the activity against tetracycline as 118.8 and 12.8-fold that of the SnS2

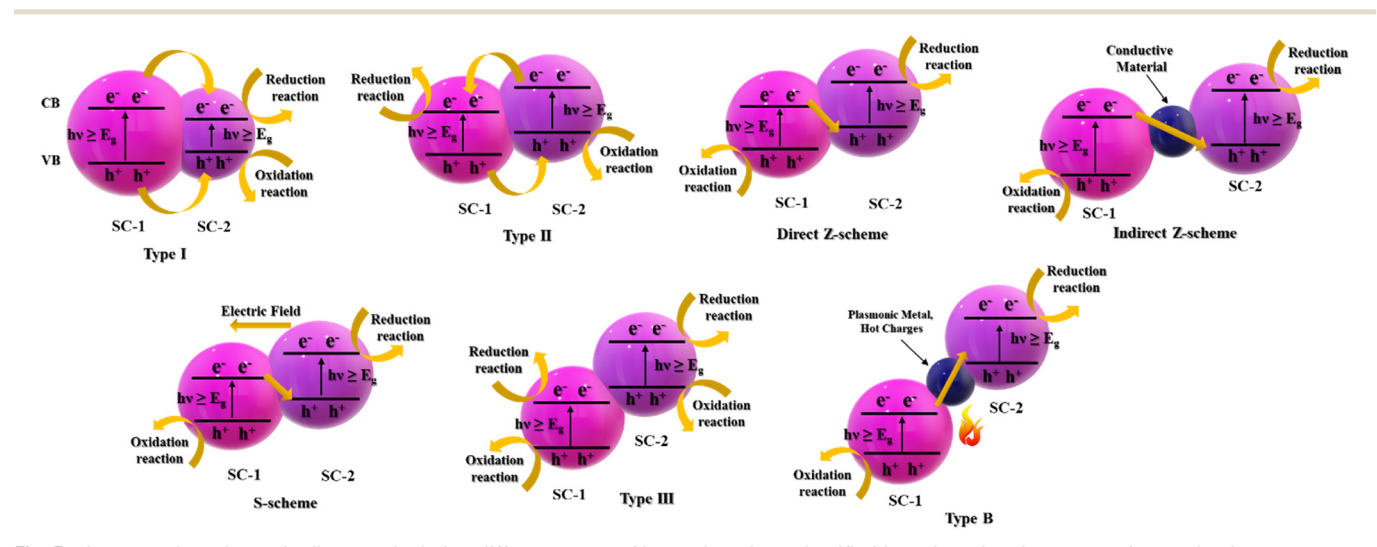


Fig. 5 A composite schematic diagram depicting different types of heterojunctions classified based on the charge transfer mechanism.

and In₂S₃, respectively. Liu et al. synthesized the BiVO₄/Bi₂₅-VO₄₀ composite material via an alkali-mediated dissolutionrecrystallization strategy to achieve the intimate type II heterojunction with close interfacial contact. The obtained heterojunction facilitated effective charge transfer and spatial separation of the carriers, resulting in enhanced photocatalytic activity towards tetracycline.⁵⁵ Huang et al. fabricated the type II heterostructure using a zirconiumbased MOF and tungsten oxide (UiO-66-NH2@WO3) on a carbon cloth. They could remove 100% tetracycline from water within 60 min under visible light irradiation.²⁰ Recently, Li et al. developed a ferroelectric Ag₁₀Si₄O₁₃/TiO₂ type II heterojunction and studied the methylene blue degradation under visible light irradiation.⁵⁶ Various type II heterojunctions of g-C₃N₄ with different components were listed by Ong et al.26 The type II heterojunction has a drawback from a thermodynamics perspective, i.e., the improved charge separation is achieved at the expense of reduced redox potential. As the electron moves from the higher potential semiconductor component to a lower potential one, it will have a weak reduction potential, and similarly, a hole will have a weak oxidation potential with such a hopping process.⁵⁷ Subsequent studies identified several strategies to overcome this issue, which were then recognized as the sub-types of type-II heterojunctions and termed as 'Z-scheme' and 'S-scheme' based on the charge transfer mechanism.

The concept of the Z-scheme photocatalytic system was initially proposed by Bard in 1979.58-60 The Z-scheme was inspired by the natural photosynthesis in green plants where 700 and 680 nm photons are harvested using photosystems I and II (PS-I and PS-II), respectively, oxidizing H₂O to O₂ under sunlight with a quantum yield close to unity.⁶¹ This system combines two different photocatalysts through a shuttle redox mediator.

In the Z-scheme, there is electron-hole recombination between the CB and VB levels that lie at the intermittent positions. Such a scenario makes the electron and hole occupying the respective higher CB and lower VB levels available for ROS generation. This heterojunction is preferable to the type II heterojunction in that it preserves the strong reductive and oxidative abilities of the electron and the hole, respectively.⁶² A Z-scheme comprising vanadium-substituted phosphomolybdic acid clusters/g-C₃N₄ nanosheets with effective charge separation and strong redox potentials was developed by Xing et al. and was utilized for the upcycling of polyethylene, which is an unusual and crucial application.63 The squandering of plastic is a potential threat to nature and explains the eminence of the heterojunction photocatalyst in this work. The Z-scheme is further divided into two types: 'indirect Z-scheme', in which the Z-type charge transfer is achieved through an electron mediator (conductors), and 'direct Z-scheme', in which no such electron mediator is employed.⁶⁴

Several helpful review articles related to the Z-scheme charge transfer are available. Low et al. presented the Z-scheme evolution road map for photocatalytic systems from the first to third generations.⁵⁹ Comprehensive details of the direct Z-scheme and various charge transfer mechanisms, such as internal electric field, interfacial defect-induced charge transfer, and facet-induced charge transfer, have been discussed in detail by Li et al.62 Zhang et al. summarized various Z-schemes dedicated to CO2 reduction reactions.64 Maeda described the historical development of photocatalytic water splitting driven by the Z-scheme. 61 Zhou et al. provided a concise overview of all-solid-state Z-scheme photocatalytic systems, including composition, construction, optimization, and applications.65 Di et al. summarized the research progress in sulphide-based direct Z-scheme photocatalysts.⁶⁶ A review by Ng et al. described the fundamental rationales in Z-scheme water splitting and challenges in the scaling up of the process,⁶⁷ and several studies have deployed the Z-scheme for the high photocatalytic activity.⁶⁸⁻⁷¹

Despite several advancements, unwanted recombination of electrons and holes between the higher CB and lower VB levels was not fully avoided. Hence, a further sub-type, called the 'S-scheme', was introduced, in which an oxidation photocatalyst is coupled with a reduction photocatalyst. The oxidation photocatalyst has a higher oxidation potential, and the reduction photocatalyst has a higher reduction potential. The electron transfer in the S-scheme is like a 'step' from the macroscopic viewpoint and resembles the letter 'N' from the microscopic view. This novel S-scheme was discussed in detail by the synthesis of the ultrathin 2D/2D WO₃/g-C₃N₄ by Fu et al. 72 The interfacial charge transfer mechanism was investigated using ex situ and in situ irradiated X-ray photoelectron spectroscopy (XPS), electron paramagnetic resonance (EPR), and atomic force microscopy (AFM) employed in the potential mode.⁵⁷ Xia et al. fabricated an S-scheme consisting of CeO2 quantum dots and polymeric carbon nitride (PCN).73 Charge transfer via the S-scheme was validated by XPS, and EPR experimental studies, which was further supported by the density functional theory (DFT) calculations. Higher antibacterial activity toward Staphylococcus aureus was seen under illumination as a result of the improved charge transfer.

Li et al. recently fabricated the TaON/Bi₂MoO₆ core-shell S-scheme and found that the material had high photocatalytic activity towards levofloxacin removal and Cr(v1) reduction.74 The enhancement in the activity is attributed to the S-scheme heterojunction resulting in the higher charge separation efficiency and, thereby, the higher redox potential of the photogenerated charges. TiO2/CsPbBr3 hybrids were fabricated by Xu et al. for CO2 photoreduction. The enhanced CO₂ photoreduction results were attributed to the formation of the S-scheme heterojunction. DFT calculations and the experimental results confirmed the existence of the internal electric field (IEF) going from CsPbBr3 to TiO2. Upon irradiation, the IEF drives back the electrons from TiO2 to CsPbBr₃, which was confirmed by in situ XPS experiments.⁷⁵ By coupling inorganic and organic semiconductors, Cheng et al. created the S-scheme. They synthesized pyrene-alt-

Table 1 Representative literature on the type I heterojunction photocatalysts

Catalyst	Band gap (optimal catalyst, eV)	Catalyst loading	Synthesis protocol	Light source	Pollutant/activity	Pollutant/dye (conc.)	Rate constant	Ref.
Fe ²⁺ -doped ZnFe ₂ O ₄ /ZnO	1.78	1 g L ⁻¹	Two-step microwave-assisted	Sunlight	RhB	10 μΜ	0.111 min ⁻¹	81
Ni _x P/Mn ₃ O ₄ / g-C ₃ N ₄ /RP	1.96	5 mg	solvothermal Two-step photochemical deposition	300 W xenon lamp (with an AM 1.5G filter)	Hydrogen generation	10 mL of 20 vol% triethanolamine (TEOA) solution	5851.3 mmol g ⁻¹ h ⁻¹	82
$\alpha\text{-Ag}_2WO_4/Ag_3PO_4$	NA	50 mg	Coprecipitation method	Visible light	RhB	50 mL, 10 mg L ⁻¹	0.504 min ⁻¹	83
P-doped g- C_3N_4 /O-doped g- C_3N_4	NA	50 mg	Solid state synthesis	300 W xenon lamp, 420 nm cut-off filter	H ₂ O ₂ production	EtOH (5 mL) + water (45 mL)	179 μM h ⁻¹	84
$\rm NiS/ZnIn_2S_4/g\text{-}C_3N_4$	NA	100 mg	Solid state synthesis, solvothermal	300 W xenon-arc lamp intensity: 120 mW m ⁻²	H_2 generation	100 mL (80 mL deionized water and 20 mL TEOA)	5.02 mmol g ⁻¹ h ⁻¹	85
BP QD/S doped g-C $_3$ N $_4$	NA	20 mg (AAP)	Hard template-assisted solid state synthesis, ultrasound-assisted	300 W Xe lamp 420 nm cut-off filter	Amino acid production H_2 evolution	Amino acid production: 100 mL (100 mmol of lactic acid, 20 mL of 25 wt% ammonia solution, and deionized water), 45 °C under 1 bar N ₂	0.643 mmol h ⁻¹ (amino acid production)	86
		100 mg (H ₂ evo.)		IR radiation: 300 W xenon lamp with 800 nm cutoff filter		H ₂ evolution: 100 mL of the aqueous solution of 10 vol% triethanolamine (TEOA) as a sacrificial agent	102 μ mol $h^{-1} (H_2)$ production	
Ag_2O -KNb O_3	NA	30 mg	Hydrothermal, <i>in situ</i> deposition method	Visible light irradiation	Sulfamethoxazole (SMZ) degradation	SMZ (5 ppm) aqueous solution	0.0603 min ⁻¹	87
g-C ₃ N ₄ quantum dots@SnS ₂	2.13	50 mg	Hydrothermal, solid state synthesis	500 W Xe lamp	Bisphenol A (BPA)	50 mL of BPA solution (10 ⁻⁵ M)	0.472 h^{-1}	88
O-doped g- $C_3N_4/$ red P	NA	10 mg	Solid-state synthesis, mechanical griding	Xenon 300 W lamp	Malachite green (MG)	50 mL of MG aqueous solution (20 mg L ⁻¹)	0.116 min ⁻¹	89
$\beta\text{-}Ga_2O_3\text{-}TiO_2\text{-}SiO_2$	2.95	$4.0~\mathrm{g~L}^{-1}$	High temp. calcination, precipitation method, ball milling	1. UV source, 2. Visible light	p-Nitrophenol (PNP)	25 mL, 25 mg L ⁻¹	0.62 mg g ⁻¹ min ⁻¹ (UV source) and 0.53 mg g ⁻¹ min ⁻¹ (visible light)	90
PMPTA coated MIL-125(Ti)	2.9	30 mg	Solvothermal, solid state synthesis	5.0 W 420 nm LED	Selective oxidation of fluorene to fluorenone	NHPI: 0.03 mmol, acetonitrile: 6 mL, fluorene: 0.3 mmol	>99% conversion	91
Boron nitride coupled Bi ₂ MoO ₆	2.52	NA	Solid-state synthesis, solvothermal, impregnation method	Visible light	Iohexol (IOH) degradation	NA	0.0160 min ⁻¹	92

Table 1 (continued)

Band gap (optimal catalyst, eV)	Catalyst loading	Synthesis protocol	Light source	Pollutant/activity	Pollutant/dye (conc.)	Rate constant	Ref
NA	10 mg	Precipitation– exfoliation process, ultrasonication	300 W Xe lamp, cut-off filter (≥420 nm)	H ₂ generation	20 ml deionized water and 5 ml lactic acid	18.43 mmol h ⁻¹ g ⁻¹	93
2.4	NA	Solid-state synthesis, hydrothermal synthesis, green wet- impregnation method	300 W Xe lamp, 420 nm cutoff filter	Reactive blue 19 (RB19)	$250 \text{ mL},$ 20 mg L^{-1}	0.07357 min ⁻¹	94
NA	30 mg	Wet chemical synthesis, electrostatic adsorption	300 mW cm ⁻² Xe lamp ($\lambda \ge$ 420 nm)	H ₂ generation	10 ml saturated HI solution containing 20 vol% H ₂ PO ₂	3742 μmol h ⁻¹ g ⁻¹	95
NA	20 mg	Hydrothermal synthesis, impregnation	Rayonet RMR-3000, 300 nm, 4 W each with 6 in. in	Methyl orange (MO)	1 × 10 ⁻⁵ M, 20 mL	7.895 × 10 ⁻² min ⁻¹	52
1.91	10 mg	Copper plate-based wet chemical synthesis	300 W Xe lamp (L.O. TQuantum design) equipped with a cutoff filter of 395 nm	${ m H}_2$ evolution	18 mL, water: acetonitrile mixture (1:1) at room temperature, 2 mL triethanolamine is the sacrificial electron donor	34 μmol h ⁻¹ g ⁻¹	
2.65	5 mg	Multistep wet chemical synthesis, hydrothermal	300 W Xe lamp	CO ₂ photoreduction	NA	CO production rate 87.43 µmol h ⁻¹ g ⁻¹	51
	(optimal catalyst, eV) NA 2.4 NA NA 1.91	(optimal catalyst catalyst, eV) Catalyst loading NA 10 mg 2.4 NA NA 30 mg NA 20 mg 1.91 10 mg	(optimal catalyst catalyst, eV) loading Synthesis protocol NA 10 mg Precipitation—exfoliation process, ultrasonication 2.4 NA Solid-state synthesis, hydrothermal synthesis, green wet-impregnation method NA 30 mg Wet chemical synthesis, electrostatic adsorption NA 20 mg Hydrothermal synthesis, impregnation 1.91 10 mg Copper plate-based wet chemical synthesis 2.65 5 mg Multistep wet chemical synthesis,	(optimal catalyst, eV) Catalyst loading Synthesis protocol Light source NA 10 mg Precipitation— exfoliation process, ultrasonication 300 W Xe lamp, cut-off filter (≥420 nm) 2.4 NA Solid-state synthesis, hydrothermal synthesis, green wet-impregnation method 300 W Xe lamp, 420 nm cutoff filter NA 30 mg Wet chemical synthesis, electrostatic adsorption 300 mW cm⁻² Xe lamp (λ ≥ 420 nm) NA 20 mg Hydrothermal synthesis, impregnation Rayonet Rayonet Rayonet Rayonet synthesis, impregnation NA 20 mg Copper plate-based wet chemical synthesis 300 W Xe lamp (L.O. TQuantum design) equipped with a cutoff filter of 395 nm 2.65 5 mg Multistep wet chemical synthesis, lamp 300 W Xe lamp	(optimal catalyst, eV) Catalyst loading Synthesis protocol Light source Pollutant/activity NA 10 mg Precipitation— exfoliation process, ultrasonication 300 W Xe H₂ generation 2.4 NA Solid-state synthesis, hydrothermal synthesis, green wetimpregnation method synthesis, electrostatic adsorption lamp, 420 mm cutoff filter (RB19) NA 30 mg Wet chemical synthesis, electrostatic adsorption 300 mW 420 nm) H₂ generation NA 20 mg Hydrothermal synthesis, impregnation RMR-3000, impregnation (MO) NA 20 mg Copper plate-based wet chemical synthesis RMR-3000, imp (MO) (MO) 1.91 10 mg Copper plate-based wet chemical synthesis 300 W Xe lamp (L.O. TQuantum design) equipped with a cutoff filter of 395 nm H₂ evolution 2.65 5 mg Multistep wet chemical synthesis, lamp 300 W Xe lamp photoreduction	(optimal catalyst, eV) Catalyst catalyst, eV) Catalyst catalyst, eV) Catalyst conc.) Synthesis protocol Light source Pollutant/activity Pollutant/dye (conc.) NA 10 mg exfoliation process, ultrasonication 2300 W Xe lamp, cut-off filter (≥420 nm) cut-off filter (≥420 nm) 20 ml deionized water and 5 ml lactic acid 2.4 NA Solid-state synthesis, hydrothermal synthesis, green wet-impregnation method 300 W Xe lamp, 420 mm cutoff filter Reactive blue 19 lactic acid 250 mL, lamp, 20 mm cutoff filter NA 30 mg synthesis, electrostatic adsorption 420 mm cutoff synthesis, impregnation 420 nm) H₂ generation 10 ml saturated HI solution containing 20 vol% H₃PO₂ lamp (¼) lamp (¼) lamp (MO) NA 20 mg lamp, 420 mg synthesis, electrostatic adsorption 420 mm lamp (¼) lamp (½) lamp (MO) Methyl orange lamp (MO) 1 × 10⁻⁵ M, lamp (MO) NA 20 mg lamp, 420 mg lamp (MO) 300 mm, 4 lamp (LO. lamp (LO. lamp) lamp (MO) 20 mL lamp (LO. lamp (LO. lamp) lamp lamp lamp lamp lamp lamp lamp lamp	Catalyst, eV Catalyst Catalyst Catalyst Catalyst, eV Catalyst, eV Catalyst, eV Catalyst, eV Catalyst Catalyst, eV Catalyst Catalyst, eV Catalyst Catalyst, eV Catalyst Catalyst

triphenylamine (PT) decorated with CdS nanocrystals, which showed robust hydrogen evolution activity. The charge transfer mechanism was probed in detail by photoirradiated Kelvin probe measurement and in situirradiated XPS analyses.76

The selected recently published literature based on type I, II, Z-scheme, and S-scheme are presented in Tables 1-4.

Type III

The type III heterojunction resembles the heterojunction in several ways, except that the CB and VB levels are positioned so that the band gaps of the semiconductor components do not intersect. Consequently, a stronger driving force is required for the charge transfer.^{26,77} To circumvent this, the researchers employed a unique strategy of interfacing two semiconductors through metal nanoparticles to facilitate charge transfer by bridging the two components. Such a sub-type configuration was termed a 'Type B' heterojunction. Li et al. employed the 'Type B' heterojunction by introducing Ag nanoparticles (Ag NPs) into the Ag₃PO₄/GdCrO₃ type III heterojunction to enable the photothermal plasmonic resonance-assisted transfer (PTPRT) process. The study found that Ag₃PO₄/Ag/GdCrO₃ exhibited a 22-fold higher photothermocatalytic degradation rate of toluene as compared to Ag₃PO₄/GdCrO₃, besides high efficiency towards volatile organic compound degradation and CO₂ reduction. The substantial temperature and local surface plasmon resonance (LSPR) from silver nanoparticles were attributed to facilitating the ballistic transport of electrons across the PTPRT channel, leading to higher efficiency.⁷⁸ In a different investigation, the same group reported a series of type B heterojunctions, namely, CuWO₄/ Ag/GdCrO₃, WO₃/Ag/GdCrO₃, and Bi₂WO_{6-x}F_{2x}/Ag/GdCrO₃, wherein WO₃/Ag/GdCrO₃ was found to exhibit more photothermocatalytic toluene degradation and CO2 reduction as compared to the WO₃/GdCrO₃ type III heterojunction.⁷⁹ A recent study by the same group reported the formation of defect sites at the interface of WO_{3-x} and GdCrO₃ to create a type B heterojunction, which enabled storage, secondary excitation, and interband transfer of the photothermalinduced charges. The as-developed defect band bridge exhibited excellent photothermocatalytic performance for CO₂ reduction and volatile organic compound degradation.⁸⁰

In a nutshell, the various heterojunctions discussed so far have several advantages and disadvantages. Depending on

Table 2 Representative literature on the type II heterojunction photocatalysts

Paper Pape									
3.18 eV 8 mg Acidic Ac	Catalyst	Band gap (optimal catalyst, eV)		Synthesis protocol	Light source	Pollutant/activity	Pollutant/dye (conc.)	Rate constant	Ref.
NA 50 mg Phycecaure publication Phycecaure publication Phycecaure publication Phycecaure publication Phycecaure publication Phycores and concentration Of 20 mg L ⁴	Melem Nanorectangular prism-modified {Mo ₇₂ Fe ₃₀ } nanocapsule	3.18 eV		Acidic depolymerization, wet chemical synthesis, modified incipient-wetness	18 W full spectrum reptile light (LT) lamp	$ m H_2O_2$ dismutation	10 ml of an acetate buffer (0.1 M, pH = 3.0) containing 20.0 mM $\rm H_2O_2$ (20 $\rm \mu L)$	17 mg L^{-1} O ₂ evolution in 3 h	96
NA 2 mg (H ₂ O ₂ Frontile para examination 1.070 W mit ⁻²) light H ₂ O ₂ production 1.00 m method, wet chemical 1.070 W mit ⁻²) light 1.00 m method, wet chemical 1.070 W mit ⁻²) light 1.00 m method, wet chemical 1.070 W mit ⁻²) light 1.00 m method, wet chemical 1.070 W mit ⁻²) light 1.00 m method	$\mathrm{g\text{-}C_3N_4/Bi_2MoO_6}$	NA	50 mg	procedure High-energy ball-milling process and corona	300 W xenon lamp, $\lambda > 420$ nm	TC degradation	50 ml of TC solution with a concentration of 20 mg r ⁻¹	0.0045 min ⁻¹	26
2.82 eV 1.32 g L ⁻¹ Co-precipitation Visible light MB, MO, RhB 13.2 mg L ⁻¹ Co-precipitation Visible light MB, MO, RhB 13.2 mg L ⁻¹ Co-precipitation Visible light MB, MO, RhB 13.2 mg L ⁻¹ Co-precipitation Visible light MB, MO, RhB 13.2 mg L ⁻¹ Co-precipitation Visible light MB, MO, RhB 13.2 mg L ⁻¹ Co-precipitation Visible light MB, MO, Cit(vi) Cit(vi) solution MB 97% MB	Ag/starched functionalized-Co ₃ O ₄ /NiFe ₂ O ₄		$2 \mathrm{mg} \left(\mathrm{H_2O_2} \right)$	points post-treatment Hydrothermal synthesis, co-precipitation method, wet chemical synthesis	Cool white LED $(1070 \mathrm{~W~m}^{-2})$ light	$ m H_2O_2$ production	H_2O_2 production: 600 μL suspension (from 5 mL DI water +2 mg catalyst) +5 mL DI water	$\rm H_2O_2$ produced 1660 μmol $\rm g^1~h^{-1}$	86
2.82 eV 1.32 g L ⁻¹ Co-precipitation Visible light MB, MO, RhB 13.2 mg L ⁻¹ Degradation in 71 min method s ₈ /TiO ₂ NA 20 mg Hydrothermal reaction of anhydrous glucose (2 > 400 nm) Photoreduction (60 mL, 30 mg L ⁻¹) MO 64% S ₈ /TiO ₂ NA 3 cm × 5 cm Hydrothermal visible light, 300 W xe lamp, λ > TC degradation (60 mL, 20 mg L ⁻¹) min ⁻¹ C(v) (94.44%) 0.04c28 min ⁻¹ NA 3 cm × 5 cm Hydrothermal visible light, 300 W xe lamp, λ > TC degradation (10 mL, 20 mg L ⁻¹) min ⁻¹ C(v) (94.44%) 0.04c28 min ⁻¹ (RB) NA 0.1 g Hydrothermal synthesis, 300 W xe lamp, λ > TC degradation (10 mg L ⁻¹) co.0171 min ⁻¹ alkali treatment 4.00 mm 2.64 eV 30 mg Multistep synthesis 300 W xe lamp, RB, MO (10 mg L ⁻¹ , 50 mL), and hydrothermal 4.0 kHz, 120 W RB, MO (10 mg L ⁻¹ , 50 mL), and hydrothermal 4.0 kHz, 120 W RB, MO (10 mg L ⁻¹ , 50 mL), solvothermal 4.0 kHz, 120 W RB, MO (10 mg L ⁻¹ , 50 mL), bisphenol 2, and hydrothermal 4.0 kHz, 120 W RB, moderate (10 mg L ⁻¹ , 50 mL), bisphenol 2, and hydrothermal 4.0 kHz, 120 W RB, moderate (10 mg L ⁻¹ , 50 mL), bisphenol 2, and hydrothermal bisphenol 3, and hydrothermal bisphenol 2, and hydrothermal bisphenol 3, and hydrothermal bisphenol 2, and hydrothermal bisphenol 3, and hydrothermal bisphenol 3, and hydrothermal bisphenol 3, and hydrothermal bisphenol 4, and hydrothermal bisphenol 4, and hydrothermal bisphenol 4, and hydrothermal 4, and hydrothermal bisph			2 mg (TC degradation)			TC degradation	TC degradation: 600 µL suspension (from 5 mL DI water + 2 mg catalyst) + 5 mL O num ferraveline solution	TC rate is NA	
4.8 μ /Hi ² NA 20 mg Hydrothermal reaction of anhydrous glucose Hydrothermal reaction of anhydrous glucose Hydrothermal Photoreduction (60 mL, 20 mg L ⁻¹) (60 mL, 20 mg L ⁻¹) (60 mL, 20 mg L ⁻¹) (60 mL, 13 mg L ⁻¹) (60 mL, 20 mg L ⁻¹) (70 m	Carbon nanotube CNT)-modified SrTiO ₃ /Fe ₂ TiO ₅	2.82 eV	$1.32~\mathrm{g~L^{-1}}$	Co-precipitation method	Visible light	MB, MO, RhB	13.2 mg L ⁻¹	Degradation in 71 min MB 97% RhB 89% MO 64%	66
NA $3 \text{ cm} \times 5 \text{ cm}$ Hydrothermal, 300 W Xe lamp, $\lambda > 7 \text{ C}$ degradation 100 mL , 20 mg L^{-1} $\frac{\text{min}^{-1}}{1.99} \text{ eV}$ 5 mg One-step hydrothermal Visible light, 300 W RhB, TC 50 mL RhB/TC 50 mL RhB/TC 50 mL RhB/TC 50 mL RhB/TC 50 mL LkB/TC 50 mg Lizetment 4.20 nm filter 4.20 mm filter 4.20 mm filter 4.20 mm Hydrogen 80 mL of 4.00 mm 4.00 mL 4.00 mm Hydrogen 4.00 mL 4.00	Oouble-shell SnIn ₄ S ₈ /TiO ₂	NA	20 mg	Hydrothermal reaction of anhydrous glucose Hydrolysis of TBT and calcination In situ hydrothermal	250 W xenon lamp (\(\lambda > 400 nm \)	MO, Cr(v1) photoreduction		Degradation in 60 min MO (90.08%) 0.03005 min ⁻¹ Cr(νη) (94.44%) 0.04628	100
Solvothermal solvothermal visible light, 300 W RhB, TC $= 50 \mathrm{mL} \mathrm{RhB/TC}$ $= 0.1716 \mathrm{min}^{-1} (\mathrm{RhB})$ $= 0.09 \mathrm{eV}$ $= 1.99 \mathrm{eV}$ $= 1.9$	UiO-66-NH ₂ -WO ₃	NA		Hydrothermal,	300 W Xe lamp, $\lambda >$	TC degradation		min ⁻¹ 0.0402 min ⁻¹	20
NA 0.1 g Hydrothermal synthesis, 300 W Xe lamp, λ > TC degradation 100 mL TC, 30 mg L ⁻¹ 0.01071 min ⁻¹ alkali treatment 420 nm 2.64 eV 30 mg Multistep synthesis 300 W Xe lamp Hydrogen 80 mL of a 10 vol% 2.07 \pm 0.03 mmol g ⁻¹ h ⁻¹ generation TEOA aqueous solution containing H ₂ PtCl ₆ NA 0.1 g Wet chemical synthesis Ultrasonic vibration, RhB and hydrothermal 40 kHz, 120 W And (10 mL, 10 ppm and hydrothermal 300 W Xe lamp phenol, MO (10 mg L ⁻¹ , 50 mL), bisphenol B, and bisphenols bisphenol Z (10 mg L ⁻¹ , 50 mL)	snS ₂ /In ₂ S ₃	1.99 eV	5 mg	solvothermal One-step hydrothermal	400 nm Visible light, 300 W Xe lamp, UV cutoff	RhB, TC degradation	50 mL RhB/TC (10 mg L^{-1})	0.11716 min ⁻¹ (RhB) 0.04280 min ⁻¹ (TC)	54
2.64 eV 30 mg Multistep synthesis 300 W Xe lamp Hydrogen 80 mL of a 10 vol% 2.07 ± 0.03 mmol $g^{-1}h^{-1}$ generation TEOA aqueous solution containing H_2 PtCl ₆ NA 0.1 g Wet chemical synthesis, and hydrothermal and hydrothermal and hydrothermal 40 kHz , 120 W RhB, MO, RhB (5 mg L^{-1} , 50 mL), solvothermal solvothermal hydrothermal h	$\mathrm{BiVO_4/Bi_{25}VO_{40}}$	NA	$0.1 \mathrm{g}$	Hydrothermal synthesis, alkali treatment	300 W Xe lamp, $\lambda > 420$ nm	TC degradation	100 mL TC, 30 mg $\rm L^{-1}$	0.01071 min ⁻¹	22
NA 0.1 g Wet chemical synthesis Ultrasonic vibration, RhB 100 mL, 10 ppm 0.067 min ⁻¹ and hydrothermal 40 kHz, 120 W NA 50 mg Two step synthesis, 300 W Xe lamp phenol, MO (10 mg L ⁻¹ , 50 mL), bisphenol R, and bisphenols bisphenols (10 mg L ⁻¹ , 50 mL) bisphenol Z (10 mg L ⁻¹ , 50 mL)	Nb ₂ O ₅ /g-C ₃ N ₄	2.64 eV	30 mg	Multistep synthesis	300 W Xe lamp	Hydrogen generation	80 mL of a 10 vol% TEOA aqueous solution containing H ₂ PtCl	$2.07 \pm 0.03 \text{ mmol g}^{-1} \text{ h}^{-1}$	101
NA 50 mg Two siep synthesis, 300 W Xe lamp RhB, MO, RhB (5 mg L^{-1} , 50 mL), 0.1606 min ⁻¹ solvothermal phenol, MO (10 mg L^{-1} , 50 mL), bisphenol A, phenol (10 mg L^{-1} , 50 mL) bisphenol B, and bisphenols bisphenols L^{-1} , 50 mL)	OdS/SpO	NA	0.1 g	Wet chemical synthesis and hydrothermal	Ultrasonic vibration, 40 kHz. 120 W	RhB	100 mL, 10 ppm	0.067 min ⁻¹	102
	//Biolo ₃ /[Bi ₆ O ₆ (OH) ₃] NO ₃) ₃ ·1.5H ₂ O [//BiolO ₃ /BHN]	NA	50 mg	Two step synthesis, solvothermal	300 W Xe lamp	RhB, MO, phenol, bisphenol A, bisphenol B, bisphenol Z	RhB (5 mg L^{-1} , 50 mL), MO (10 mg L^{-1} , 50 mL), phenol (10 mg L^{-1} , 50 mL) and bisphenols (10 mg L^{-1} , 50 mL)	0.1606 min ⁻¹	103

This article is licensed under a Creative Commons Attribution-NonCommercial 3.0 Unported Licence. Open Access Article. Published on 27 Fankwa-b 2023. Downloaded on 2025/10/19 12:09:36 PM.

_
ģ
æ
2
≊
2
õ
\circ
~
ø
<u> </u>
<u>a</u>
_

(5)5:::::::::::::::::::::::::::::::::::								
	Band gap (optimal catalyst,	Catalyst						
Catalyst	eV)	loading	Synthesis protocol	Light source	Pollutant/activity	Pollutant/dye (conc.)	Rate constant	Ref.
Magnetic 3-D ZnFe₂O₄/ZnO aerogel	1.9 eV	50 mg	Aerogel formation, calcination	300 W xenon lamp (PLS-SXE300/300UV) with a 400 nm cut-off filter	Cr(v) reduction	100 mL $Cr(v_1)$ solution with the initial $Cr(v_1)$ concentration value of 100 mg L^{-1} . 1 mL HCOOH, as the hole trapping agent, pH 2	$87.0 \times 10^{-3} \text{ h}^{-1}$	104
$\mathrm{Ag_{10}Si_4O_{13}/TiO_2}$	NA	20 ppm of ASO/TO (2: 1) catalyst	Hybridization sol-gel method	300 W xenon lamp, with an ultraviolet filter $(\lambda > 420 \text{ nm})$	MB degradation	5 ppm	0.1147 min ⁻¹	26
Co-doped 3D petal-like ZnIn ₂ S ₄ /GaN	NA	Thin film (15 × 30 mm)	MOCVD (metal-organic chemical vapor deposition), hydrothermal	300 W Xe lamp, filter to cut off the light below 400 nm	Chlortetracycline degradation	$50~\mathrm{mL}, 20~\mathrm{mg~L^{-1}}$	$0.00503 \; \mathrm{min^{-1}}$	105
h-BN/flower-ring g- C_3N_4	NA	20 mg	Thermal polymerization	300 W xenon lamp and filtered by a 420 nm filter	TC degradation	$100~\mathrm{mL},20~\mathrm{mg}~\mathrm{L}^{-1}$	0.0703 min ⁻¹	106
$\mathrm{SnS_2/Bi_2WO_6}$	NA	120 mg	Hydrothermal, ultrasonication and thermal treatment route	44 W LED, 5.3 mW cm $^{-2}$, $\lambda > 400$ nm	Glyphosate degradation tests	$300~\mathrm{mL}$ of $10^{-4}~\mathrm{mol}~\mathrm{L}^{-1}$	0.0065 min ⁻¹	107
$\mathrm{Bi} @ \mathrm{H^{\text{-}}Ti} \mathrm{O}_{2} / \mathrm{B\text{-}} \mathrm{C}_{3} \mathrm{N}_{4}$	NA	20 mg	Solvothermal, calcination, thermal polymerization	300 W Xe lamp covered by cutoff filter	$ m H_2$ production	30 mL of triethanolamine aqueous solution (20 vol%, sacrificial agent)	$\lambda > 300$ nm irradiation: 223.08 µmol g^{-1} h ⁻¹ under visible light ($\lambda > 400$ nm): 18.84 µmol g^{-1} h ⁻¹	108
CeO ₂ /MIL-101(Fe)	NA	30 mg	Hydrothermal calcination, solvothermal	300 W xenon lamp with a 420 nm cut-off filter	TC degradation	$100~\mathrm{mL},20~\mathrm{mg}\mathrm{L}^{-1}$	TC degradation: 83.5%, 120 min	109
CeO _x /In ₂ O ₃	2.43 eV	50 mg	Hydrothermal, wet impregnation	500 W xenon arc lamp	CO ₂ photoreduction	CO ₂ (99.999%) and CH ₄ (99.995%), 0.3 bar above atmospheric pressure, the feed ratio of CO ₂ and CH ₄ was maintained at 1.0	CO and H ₂ produced 79 and 158 µmol g _{cat} ⁻¹ in 5 h	110
CdS/Cd-MOF	2.29 eV	10 mg	Solvothermal	Xenon lamp irradiation (200 W, $\lambda = 320-1100 \text{ nm}$)	MB degradation	$100 \ \mathrm{mL} \ \mathrm{MB} \ (20 \ \mathrm{mg} \ \mathrm{L}^{-1})$	$0.023~\mathrm{min}^{-1}$	111
${ m ZnWO_4/SnS_2}$	2.37 eV	Cr(vı) 50 mg TC 30 mg MB 30 mg	Hydrothermal synthesis	Under sunlight exposure	MB, TC, Cr(v1) reduction	100 mL of Cr(v _I) (50 mg L ⁻¹), pH 2.5 50 mL of TC (20 mg L ⁻¹) 50 mL of MB (20 mg L ⁻¹)	Cr(vr): 0.061 min ⁻¹ TC: 0.023 min ⁻¹ MB: 0.055 min ⁻¹	112
								•

these factors, they can be employed for suitable applications with the wise choice and combination of various materials discussed in the 'Library of materials used for heterojunction formation in photocatalysis' section. A Schottky barrier can be deployed where the unilateral flow of electrons in forward-biased direction is required, resulting in efficient charge separation. However, in ohmic contacts, the electron flow in forward and reverse-biased directions can be obtained, eventually resulting in poor charge separation and photoresponse. In this scenario, p-n junctions can offer efficient charge separation and collection.

van der Waals heterojunction can provide interlayer electron transfer in 2D materials for improved photocatalytic activity. Moreover, photogenerated charge kinetics can be stimulated by building an internal electric field in 2D materials. The facet heterojunction is a relatively different form of heterojunction; usually, in heterojunctions, two components are involved but with facet heterojunctions, a single component with two different facets with a suitable energy match can be deployed to form the heterojunction as discussed earlier. The type I heterojunction has several disadvantages such as low charge separation and a lower band gap component, which will have charge accumulation and a compromised redox potential. Compared to the type I heterojunctions, the type II heterojunctions are superior due to effective charge separation and uniform charge distribution in both components; however, there will be a compromise in terms of the redox potential of the excitons. For a high redox potential, the Z-scheme is a suitable alternative; however, charge recombination is not completely averted, so the S-scheme is the preferred option with enhanced separation efficiency and light absorption. The higher efficiency due to the photothermal plasmonic resonance-assisted transfer (PTPRT) process can be achieved using a type III heterojunction.

The detailed charge transfer mechanism is of utmost importance for the effective fabrication of the heterojunction and can be studied in detail using ultrafast transient absorption microscopy, as discussed in the following section.

Detection of carrier transport across heterojunctions

The heterojunction is widely used in photocatalysis, as discussed above, and is an essential phenomenon in catalysis and optoelectronic devices. The understanding of the charge energy transport across semiconductor the heterojunction is of great importance for the effective application of heterojunctions in catalysis and various optoelectronic devices. The charge dynamics and transport across the heterojunction can be investigated using 'ultrafast transient absorption microscopy (TAM)'. By deploying such techniques, the carrier diffusion of the individual material through the interface can be visualized. TAM investigation directly quantify charge transmission through heterostructures. Such investigations have revealed that around 20% of the carrier population is lost due to interfacial

barriers and defect recombination. Detailed investigations of various reported heterojunctions using TAM give information on the efficiency heterojunction. 143-145 Moreover, an in situ dynamic study can reveal critical parameters such as the lifetime of the excited state, hole trapping and interfacial electron transfer. 146

Library of materials used for heterojunction formation in photocatalysis

The recent trends in materials used to create heterojunctions for photocatalysis are detailed below. Various classes of materials are briefly addressed with illustrative instances, while their categorization by the mechanistic heterojunction is provided in Tables 1-4.

Metal oxides

After the pioneering works by Muller, Honda, and Fujishima, various photocatalytic systems based on TiO2 and several other oxides were developed. 7,8,147-152 AEROXIDE TiO2 P25 is often considered the 'gold standard' in photocatalysis, which possesses a heterojunction between anatase and rutile polymorphs. The marketed anatase to rutile weight ratio is 80:20. 153,154 Since then, metal oxides have been front liners in photocatalysis owing to their high chemical stability and non-toxicity. Several oxides such as Fe₂O₃, WO₃, CuO, Bi₂O₃, SnO, ZrO2, V2O5, and Ni2O3 are frequently used in photocatalysis. 4,155-163 Kannan *et al.* provided a brief historical overview of nanostructured metal oxides and their used composites in photocatalytic and applications. 164 A detailed discussion on the regulation of the physiochemical properties of metal oxide nanomaterials was given by Chen et al. 165

Perovskites

Perovskites (ABX₃) are another class of materials that are routinely deployed for photocatalytic applications. The commonly used perovskites for photocatalysis are LaFeO₃, LaMnO₃, LaCoO₃, SrTiO₃, BaTiO₃, BiFeO₃, CaTiO₃, etc. ^{166–168} More details regarding the perovskites for photocatalysis are given by Schanze et al. 169 Due to their superior performance in solar cells and LED devices, metal halide perovskites have recently gained a lot of attention as a novel class of material. Various organic-inorganic and all-inorganic metal halide perovskites, such as CH₃NH₃PbX₃ and CsPbX₃, (X = Cl, Br, I), have emerged as potential candidates for different photocatalytic reactions. The exciting features of the metal halide perovskite are the redox potentials of the photogenerated holes and electrons, which can be tuned by changing the halogens. Moreover, when the size of the metal halide perovskite is smaller than the Bohr radius, it shows the multiexciton generation effect and hence supplies adequate charge carriers for multielectron redox reactions. Wang et al. provided a comprehensive review of the metal

Review

 Table 3
 Representative literature on the Z-scheme type photocatalysts

Catalyst	Band gap (optimal catalyst, eV)	Catalyst loading	Synthesis protocol	Light source	Pollutant/activity	Pollutant/dye (conc.)	Rate constant	Ref
ZnS/ZnO nanosheets	2.17 eV	50 mg	Solvothermal synthesis, heat treatment	UV light	Cr(vi) reduction, H ₂ generation	Cr VI (Pot. dichromate 100 mg L ⁻¹)	500 μmol h ⁻¹ g ⁻¹ , Cr(vι) reduction 0.0078 min ⁻¹	113
NiO/α - MoO_3	NA	0.01 g	Hydrothermal synthesis	500 W Xe lamp	MB degradation	100 mL, 10 mg $\rm L^{-1}$	0.02685 min ⁻¹	114
AgInS ₂ /AgIn ₅ S ₈ QDs	2.05 eV	0.05 mg mL^{-1}	Hydrothermal synthesis	300 W Xe light, $\lambda >$ 400 nm	Cr(vi) reduction	25 mL, 10 mg mL ⁻¹	2.01908 min ⁻¹ mol ⁻¹	115
${ m CaTiO_3/Cu/TiO_2}$	3.37 eV	30 mg	Two step hydrothermal	300 W Xe lamp, 300–1100 nm	Hydrogen generation	30 mL solution of 20 vol% MeOH, 80 vol% DW	23.550 mmol g ⁻¹ h ⁻¹	116
$CoTiO_{3}/Zn_{0.5}Cd_{0.5}S$	2.33 eV	10 mg, 25 mg (H ₂ production integrated with biomass derivative oxidation study)	Multistep synthesis	LED 3 × 30 W bulb, lambda max 450 nm	Hydrogen generation	40 mL aqueous solution of sacrificial electron donor (15 vol% lactic acid or 0.25 M Na ₂ S/0.35 M Na ₂ SO ₃) furfuryl alcohol (2 mg mL ⁻¹), 20 mL DI water	1929 μmol $g^{-1} h^{-1}$	117
g - C_3N_4/MoO_{3-x}	NA	0.05 g	Hydrothermal, two-step calcination	300 W Xe lamp	Hydrogen generation	100 mL of 10 vol% TEOA aqueous solution	209.2 μmol h^{-1}	118
$\rm Ag/WO_3/g\text{-}C_3N_4$	NA	40 mg L ⁻¹	Multistep synthesis, hydrothermal, calcination, photoreduction	500 W Xe lamp, 420–800 nm	Oxytetracycline hydrochloride	10 mg L ⁻¹	0.1164 min ⁻¹	119
$\rm TiO_2@C/g\text{-}C_3N_4$	2.69 eV	0.2 g	One step calcination	500 W Xe lamp, 420 nm cut-off filter	NO removal	100 ppm NO, 8% N_2 /air balance, 200 mL min $^{-1}$	NA	120
V-substituted phosphomolybdic acid/g-C ₃ N ₄	NA	10 mg	Self-assembly strategy	300 W Xe lamp, 420 nm cut-off optical filter	Upcycling of various plastic wastes into high-value-added formic acid	10 mL acetonitrile, 20 mg of polyethylene	$g^{-1} h^{-1}$	63
Carbon dot decorated g-C ₃ N ₄ /TiO ₂	2.70 eV	50 mg	Simple burning, hydrothermal,	Four LED lamps (3 W, 420 nm)	Hydrogen generation	80 mL triethanolamine aqueous solution (10 vol%), 34 μL H ₂ PtCl ₆ , pH 11	$580 \ \mu mol \ h^{-1} \ g^{-1}$	121
${\rm Bi}_2{\rm WO}_6/{\rm InVO}_4$	NA	0.1 g	Hydrothermal synthesis	300 W xenon arc lamp with a 420 nm cut-off filter $\lambda >$ 420 nm	CO_2 reduction	5 mL deionized water, high-purity CO ₂ with a steady flow	CO evolution rate: 17.97 μ mol g ⁻¹ h ⁻¹ , CH ₄ production rate: 1.13 μ mol g ⁻¹ h ⁻¹	122
Oxygen-doped carbon nitride/nitrogen-doped carbon dots/bismuth tetroxide	NA	0.05 g	Hydrothermal synthesis, solid state synthesis	300 W Xe lamp equipped with a UV cut-off filter	TC, MO	100 mL of TC or MO (10 mg L^{-1})	TC 0.07 min ⁻¹ MO 0.304 min ⁻¹	123
Ag-ZnO/Bi ₂ Sn ₂ O ₇	NA	50 mg	Hydrothermal synthesis,	300 W Xe lamp	TC	10 mg L ⁻¹	$0.023 \\ \text{min}^{-1}$	124

Table 3 (continued)

Catalyst	Band gap (optimal catalyst, eV)	Catalyst loading	Synthesis protocol	Light source	Pollutant/activity	Pollutant/dye (conc.)	Rate constant	Ref
			ultrasonication, photodeposition	with a 420 nm UV-cutoff filter				
${\rm CQD/Bi_{12}O_{17}C_{l2}/NiAl\text{-}LDH}$	3.14 eV	50 mg	Hydrothermal, precipitation	300 W xenon arc lamp and a 3 AM 1.5 G filter	CO_2 reduction	100 mL of deionized water, saturation with pure CO_2 at 100 kPa for 30 min	CO yield: 16.4 µmol g ⁻¹ h ⁻¹	125
$\mathrm{Bi}_{12}\mathrm{O}_{15}\mathrm{C}_{16}/\mathrm{InVO}_4$	NA	40 mg	Hydrothermal, calcination	LED 450 nm	TC, RhB	100 mL, RhB (10 mg $\rm L^{-1})$ or tetracycline TC (20 mg $\rm L^{-1})$	TC: 0.01929 min ⁻¹ RhB: 0.03712 min ⁻¹	126
MnIn $_2$ S $_4$ nanosheets/rods-like β -MnO $_2$	NA	15 mg	Hydrothermal, in situ wet chemical synthesis	350 W xenon lamp $\lambda >$ 420 nm	Cr(vi)	20 mL Cr(v _I) containing solution (50 mg L ⁻¹ , pH = 5.6 \pm 0.1)	0.05814 min ⁻¹	127

halide perovskites employed for photocatalytic H₂ evolution, CO₂ reduction, organic transformation, and organic pollutant degradation.¹⁷⁰

Chalcogenides

Chalcogenides are widely recognized for their small band gap energy and are composed of at least one chalcogen (S 2 -, Se 2 -, or Te 2 -). Due to their non-toxicity, biocompatibility, affordability, and ease of synthesis, they have received much research attention. Depending on the number of elements in the composition, the chalcogens are generally classified broadly as binary (e.g., ZnS, CuS, Cu₂Se, Ag₂Se, etc.), ternary (e.g., Zn_{0.5}Cd_{0.5}S, Ba₂ZnSe₃, BaAu₂S₂, CuFeS₂, etc.) and quaternary (e.g., Cu₂FeSnS₄, Cu₂ZnSnSe₄, etc.). Various heterostructures have been reported for photocatalytic activity (Ag/Ag₂S/CuS, Ag₂S/AgInS₂, AgInS₂ quantum dots/In₂S₃, etc.). The review by Rahman et al. discusses recently discovered chalcogenides for photocatalysis.¹⁷¹ The progress on the wide band gap chalcogenide (band gap, $E_g > 2$ eV) was summarized in detail by Woods-Robinson et al.¹⁷²

Besides the abatement of organic pollutants, the field of organic transformations employing photocatalysis is also a fascinating avenue. The commercially available CdSe photocatalyst, Muralirajan *et al.* demonstrated the highly selective trifluoromethylation of (hetero) arenes and alkenes. The theoretical simulation predicts that Janus XMMX' monolayers of group III chalcogenides are suitable for photocatalytic water splitting. Among them, SGa₂Te, SeGa₂Te, SIn₂Te, and SeIn₂Te monolayers are direct gap semiconductors, with the band gap ranging from 1.54 to 1.91 eV. These monolayers exhibit better visible light absorption and suitable band edge positions for photocatalytic water splitting. The review by Chen *et al.* provides a thorough

overview of multinary metal chalcogenides with tetrahedral structures and their uses in photocatalysis, photovoltaics, and second-order nonlinear optical applications.¹⁷⁵

The compounds with the MQX stoichiometry, where M = As, Sb, and Bi; Q = O, S, Se, and Te; and X = F, Cl, Br, and I, are known as heavy pnictogen chalcohalides. Pnictogen chalcohalides are a family of compounds with a wide band gap and a layered or chain-like structure. They are synthesized by a straightforward synthetic process and are stable. Their electrical and optical properties can be tuned by halogen or chalcogen exchange. The chalcopyrites, kesterites, and chalcohalides are relatively less explored as compared to the perovskites but their structure and properties are well-suited for photocatalysis and other applications. 176

MOFs and COFs

MOFs are a class of crystalline, extremely porous organicinorganic hybrid materials. By selecting the appropriate metal node and organic linker, the MOF's framework structure, functionality, and porosity may be adjusted. With their straightforward amalgamation of metal nodes and organic linkers, MOFs exhibit extraordinary characteristics. As a result, they are frequently employed in a variety of biological and energy-related applications, as well as in processes.177 separation researchers are showing interest in creating MOFs with two metal ions, which provide additional functionality. The bimetallic MOFs utilized for various purposes have been outlined by Manan Ahmed.178 Similar to MOFs, COFs have also been gaining popularity in recent times. They form a three-dimensional network and are majorly governed by both covalent and non-covalent interactions; covalent bonds control the primary-order chain structure, and non-covalent

Review

Catalyst	Band gap (optimal catalyst)	Catalyst loading	Synthesis protocol	Light source	Pollutant/dye	Pollutant/dye (conc.)	Rate constant	Ref.
SnS ₂ /RGO/g-C ₃ N ₄	NA	10 mg	Photoassisted self-assembly	300 W Xe lamp, cutoff filter: 420 nm $< \lambda <$ 780 nm	RhB, H ₂ generation	50 mL, 10 mg L ⁻¹	0.55 min ⁻¹	128
CdS QDs/Bi ₂ WO ₆	NA	0.2 g	Hydrothermal synthesis	PLS-SXE 300 Xe-lamp	Ethylene	50 μL	0.384 min ⁻¹	129
$\mathrm{Co_9S_8/In_2O_3}$	NA	10 mg	Solution synthesis, high-pressure reactor, hydrothermal synthesis	5 W white light, 420 nm or above	Hydrogen generation	20 mg Eosin Y, 30 mL sacrificial reagent aqueous solution (15 vol% TEOA)	277.77 μmol in 5 h	130
NH ₂ -UiO-66/SiC	NA	20 mg	Microwave synthesis	300 W Xe lamp, $\lambda >$ 420 nm	CO ₂ reduction	0.084 g NaHCO ₃ , 0.3 mL H ₂ SO ₄ (aq 2 M)	7.30 $\mu mol\ g^{-1}$ h^{-1}	131
CdS QDs/Bi ₂ MoO ₆	NA	0.2 g	Hydrothermal synthesis	Xe lamp	Ethene	50 μL	0.06036 min ⁻¹	132
$In_4SnS_8/Cs_3Bi_2Br_9$	NA	10 mg	Wet chemical synthesis, <i>in situ</i> hydrothermal	300 W argon lamp (λ > 420 nm)	CO ₂ reduction	99.999% pure CO ₂ gas inside the vessel at 80 kPa	CO yield: 9.55 μmol g ⁻¹ h ⁻¹	133
NiIn LDH/In ₂ S ₃	1.36 eV	5 mg	Wet chemical synthesis, hydrothermal	300 W Xe lamp	CO ₂ reduction	Ultra-pure CO ₂ (>99.999%)	CO yield: 29.43 µmol g ⁻¹ h ⁻¹	134
Co ₂ P/PC- <i>b</i> -TiO ₂	3.07 eV	50 mg	Hydrothermal synthesis, calcination	300 W Xe lamp, with a standard AM 1.5 filter	Hydrogen generation	100 mL of a mixed solution containing distilled water and TEOA with volume ratio of 9:1	1.53 mmol g ⁻¹ h ⁻¹	135
O-doped $\begin{array}{l} \text{O-doped} \\ \text{g-C}_3\text{N}_4/\text{N-doped} \\ \text{Nb}_2\text{O}_5 \end{array}$	2.81 eV	NA	One-step polymerization, hydrothermal synthesis, surface charge-induced hetero-aggregation	300 W xenon lamp	CO ₂ reduction	0.12 g of NaHCO ₃ , 0.35 M HCl for the <i>in</i> <i>situ</i> production of CO ₂ and H ₂ O gas	Production rates CO: 253.34 μmol g ⁻¹ h ⁻¹ CH ₄ : 68.11 μmol g ⁻¹ h ⁻¹	136
$\begin{array}{l} 0 D/3 D \\ Bi_3 Ta O_7/Zn In_2 S_4 \end{array}$	NA	50 mg	Hydrothermal, two-step solvothermal method	300 W Xe lamp with a 420 nm cut-off filter (λ > 420)	TC degradation, simultaneous H_2 generation	100 mL TC solution (10 mg L ⁻¹)	TOC removal efficiency of 36% after 180 min H ₂ evolution: 13.7 µmol g ⁻¹ h ⁻¹	137
$\rm ZnIn_2S_4-NiSe_2/Ti_3C_2$	NA	2 mg	Hydrothermal synthesis, wet chemical synthesis	Xe lamp (300 W, λ > 420 nm) with a 420 nm cut-off filter	Hydrogen generation	80 mL ascorbic acid aqueous solution (80 mL, 1.73 wt%) anaerobic environment	23.51 mmol g ⁻¹ h ⁻¹	138
Hexameric AgBr/Zn–Al MMO	NA	20 mg	Wet chemical synthesis, <i>in situ</i> co-precipitation	Xenon lamp (Perfect Light, Microsolar300, 320–780 nm, 100 mW cm ⁻² equipped with a UVIR cut 420 quartz coated filter)	TC, MO, MB	100 mL TC solution (10 mg L^{-1})	TC removal rate 95% within 60 min	139
$Zn_3In_2S_6/Bi_2O_3$	NA	50 mg	Hydrothermal synthesis	300 W Xe lamp ($\lambda >$ 400 nm)	Metronidazole, Cr(vi)	10 mg L ⁻¹ , pH 5	Metronidazole 0.0389 min ⁻¹ , Cr(vI) 0.05409 min ⁻¹	140
TiO ₂ –X/BiOI	NA	0.05 g	Sol-gel, solvothermal, solid state synthesis	PLS-SXE300C xenon lamp using AM 1.5 (λ = 300–800 nm)	H ₂ generation	100 mL of 15 vol% aqueous methanol, 1 wt% Pt by <i>in situ</i> photo deposition	804.30 µmol g ⁻¹ h ⁻¹	141

Table 4 (continued)

Catalyst	Band gap (optimal catalyst)	Catalyst loading	Synthesis protocol	Light source	Pollutant/dye	Pollutant/dye (conc.)	Rate constant	Ref.
ZnO/COF	NA	0.5 g L ⁻¹	Precipitation reaction, wet chemical synthesis, electrostatic self-assembly	300 W xenon lamp (AM 1.5, 45 mW cm ⁻²)	H ₂ O ₂ production	Aqueous ethanol (10 vol%) as an electron donor	2443 μmol g ⁻¹ h ⁻¹	142

forces create the morphology in the system. The reader is encouraged to go through the extensive assessment of COFs by Geng *et al.*¹⁷⁹

The available synthetic methods for the fabrication of the MOF/graphene heterojunction for electrocatalysis and photocatalysis have been summarized by Wang et~al., and g-C₃N₄/MOF-based heterojunctions are outlined by Zhang et~al. MOFs deployed for photocatalysis under visible light illumination have been summarized by Wang et~al. The versatile synthesis of MOF-based coatings for broad applications was reviewed by Meng et~al.

Several properties of the MOFs and COFs, such as high surface area, a defined pore structure, and several adsorption sites, make MOFs and COFs ideal components for adsorption control in photocatalysis. Moreover, several organic ligands are highly useful for the various functionalizations to control light harvesting properties in the region of interest of the entire light spectrum. These make MOFs and COFs ideal candidates for photocatalysis. 184

Many physical and chemical properties shown by the metal ions are of immense importance for various applications. Since COFs do not exhibit such characteristics, metalated COFs are often fabricated to induce the desired properties. All the aspects of such metalated COFs can be found in the review by Guan *et al.*¹⁸⁵ Comprehensive reviews of various COF catalysts deployed for photocatalytic and electrocatalytic carbon dioxide reduction are available in the literature. ^{186,187} Considerable reviews in the field of COFs are available for energy and environmental applications. ^{179,188–196}

MOF/COF heterostructures have better properties than solo MOFs and COFs because of synergism. As a result, MOF/COF-based hybrids have seen rapid advancement and have been attracting growing attention in recent years. The design principles, synthetic methods, assembly procedures, and applications of the MOF/COF-based hybrids have been thoroughly reviewed by Guo *et al.*¹⁹⁷ Various composites of the COF, such as COF/MOF, COF/g-C₃N₄, and COF/metal-semiconductors, have been studied by Hu *et al.*¹⁹⁸

MXenes

Since their discovery, MXenes have been widely studied for various applications. Exceptional properties such as thermal and electrical conductivity and a large surface area make MXenes suitable for different applications, including

bioapplications and heterojunction formation. The preferred notation for MXenes is $M_{n+1}X_nT_x$, where 'M' stands for early transition metals (Ti, Sc, Zr, Hf, *etc.*), 'X' for carbon or nitrogen, and ' T_x ' represents the terminal groups like F, Br, O, S, and OH. To date, a variety of MXenes have been fabricated, including Ti_3C_2 , Ti_2C , and Nb_2C . ^{200,201}

The large specific surface area and suitable optical and electronic characteristics make MXenes the most promising emerging materials in the field of photocatalysis. Moreover, good conductivity due to conducting nuclei in multilayer structures and various terminating functional groups makes MXenes promising photocatalysts.²⁰²

Comprehensive details on MXene-based photocatalysts have been reported by You *et al.*²⁰³ Jin *et al.* have reviewed the various heterostructures of MXenes and transition metal chalcogenides such as SnS, NiS, MoS₂, FeS₂, and NiSe₂ with special emphasis on surface/heterointerface engineering for various applications such as batteries, supercapacitors, electrocatalysis, and photocatalysis.²⁰⁴ Several 2D and 3D MXenes have been explored and summarized in multiple reviews.^{205–210}

Carbides and nitrides

Binary and ternary phases of metal carbides and nitrides are intriguing for catalytic applications. They are frequently discussed together due to their structural resemblance. The binary phases can generally be described by the location of C or N within the interstitial sites of close-packed metal lattices. It is claimed that carbides and nitrides are more resistant to poisoning, though not always, as compared to noble metals.211 Zhang et al. reported the recovery of SiC from a silicon waste slurry and found that it mainly consisted of 3C-SiC and 6H-SiC, with the surface primarily consisting of silicon oxycarbides.212 The as-recovered SiC was proved to be a promising photocatalyst for hydrogen production. The carbides of molybdenum, such as Mo₂C, MoC₂, MoC, etc., are important candidates due to their similar electronic structure to the noble metal platinum, which is highly useful for photocatalytic hydrogen production. Moreover, molybdenum carbides show remarkable properties such as adsorption, desorption, activation, and the ability to transfer hydrogen. Mo₂C forms an effective heterojunction with CdS and promotes the charge separation, resulting in the enhancement in the photocatalytic activity. 213 Porous silicon

carbide has been used widely as summarized by Tuci et al. 214 Other carbides such as niobium carbide, 215 boron carbide, 216 tungsten carbide, 217-221 silicon carbide, 222-227 vanadium carbide, 228 and titanium carbide 229 have also been reported for photocatalytic applications.

Almost all metals can combine to form a binary nitride, except for noble metals and alkali metals other than lithium. There are several known ternary and quaternary inorganic nitrides, which are considered "synthetic" materials since they do not exist in nature due to their thermodynamic instability towards oxidation. Co2N was used as a co-catalyst in the Co₂N/BiOBr system by Di et al. towards photocatalytic CO2 reduction. 230 It was shown that Co2N could interact strongly with BiOBr electrically, promoting the efficient flow of electrons from BiOBr to Co2N and to the surface. Liu et al. fabricated one-dimensional Co₄N-WN_x-CdS composites by a simple yet efficient electrostatic self-assembly. The resulting catalyst showed high conductivity and was enriched with active sites, resulting in a high rate of photocatalytic hydrogen evolution (14.42 mmol g⁻¹ h⁻¹) under vacuum conditions.231 Rao et al. discussed the overview of the nanostructured metal nitrides for photocatalytic H2 generation and CO2 reduction.232 Cheng et al. summarized recent research on transition metal nitrides.²³³ Numerous nitrides have been used in photocatalytic applications with success.234-242 GaN has been extensively studied for lightemitting device applications; however, it is now amply explored for photocatalysis as well. 243-250 Apart from the inorganic semiconductors, a polymeric nitride material, graphitic carbon nitride (g-C₃N₄), has been highly explored for photocatalysis and heterojunction formation. 251-258

Phosphides

The comprehensive synthetic strategy for various metal phosphides and their catalytic applications can be found in the review by Li et al. 259 Callejas et al. demonstrated that iron phosphide (FeP) with a uniform hollow morphology exhibited high-efficiency for the hydrogen evolution reaction both electrocatalytically and photocatalytically.260 Under UV illumination in both acidic and neutral conditions, such FeP nanoparticles deposited over TiO2 were found to exhibit H2 production at rates and amounts comparable to that of Pt/ TiO2. Ni2P and Ni12P5 were synthesized via a hydrothermal route, and the phases were controlled by varying the reaction conditions. It was observed that Ni₂P possessed high photocatalytic activity as opposed to Ni₁₂P₅.²⁶¹ The excellent synergism between ternary metal phosphides Ni_xCo_{1-x}P and Zn_{0.5}Cd_{0.5}S nanorods resulted in effective photocatalytic hydrogen production. The effective charge separation and transfer were achieved due to the coordination bonds formed on the surface of the optimized composition of Zn_{0.5}Cd_{0.5}S and Ni_{0.1}Co_{0.9}P.²⁶² The Schottky heterojunction in the MoP-Cu₃P system was reported to yield high photocatalytic activity in hydrogen generation with a production rate of 855 µmol h⁻¹ g⁻¹.²⁶³ Apart from these, several other phosphides have been explored for photocatalytic applications and used as cocatalysts.264-274

Layered double hydroxides (LDHs)

Layered double hydroxides (LDHs) or hydrotalcite-like compounds are a prominent family of 2D anionic clay materials that can be represented by the general formula $[M_{1-x}^{2+}M_x^{3+}(OH)_2]^{x+}[A_{x/n}]^{n-}\cdot mH_2O$. They are composed of brucite-like layers in which the fraction of the divalent cations (e.g., Mg²⁺, Fe²⁺, Co²⁺, Cu²⁺, Ni²⁺, or Zn²⁺) are coordinated octahedrally by hydroxyl groups. The divalent cations have been replaced isomorphously by the trivalent ones (e.g., Al3+, Cr3+, Ga3+, In3+, Mn3+, or Fe3+), giving rise to positively charged layers. The value of x is the molar ratio of $M^{2+}/(M^{2+} + M^{3+})$ and will be in the range of 0.2-0.33. The LDH can be synthesized via a simple, well-established protocol such as co-precipitation and homogeneous precipitation by urea hydrolysis.²⁷⁵

LDHs are 2D materials with various scopes for modification due to their unique layered structures. Their high adsorption capacity, tunable band gap, superior cationanion exchange capacity and separate oxidation and reduction sites make them potential photocatalysts.²⁷⁶

Zhao et al. detailed the tailoring of the electronic properties of LDH through the introduction of surface defects for the enhancement of photocatalytic properties.²⁷⁷ Highly informative review articles on LDH-based photocatalysts are available in the literature. 276,278-285

Other methods of fabricating heterojunctions

In general, a heterojunction architecture can be either a core-shell²⁸⁶⁻²⁸⁸ or a uniform blend.²⁸⁹⁻²⁹¹ Depending on the dimensions of the morphology of individual components, various 0D/1D, ^{292–296} 0D/2D, ^{297–300} 0D/3D, ^{301–304} 1D/1D, ³⁰⁵ 1D/2D, $^{306-308}$ 1D/3D, 309 2D/2D, $^{310-312}$ and $3D/2D^{313}$ heterojunctions have been reported (Fig. 6). Apart from the aforementioned methods, several other methods have been reported for synthesizing intimately mixed semiconductorbased heterojunctions, and a few representative ones from our group are presented herein.

Our group has recently developed a few synthetic strategies for obtaining intimately mixed composite materials to achieve effective heterojunctions. Composites of g-C₃N₄/ AgBr are known to exhibit good photocatalytic properties; however, the conventional synthetic procedure involves a solution-based adsorption/precipitation method that results in the particle size of AgBr in the range of 5 to 50 nm. We devised a novel single-step synthesis in which melamine (precursor of g-C₃N₄) was intimately mixed with a tetraoctylammonium bromide-Ag complex (AgBr precursor). This solid-state approach utilized the thermal decomposition of the physically grounded precursor mixtures to obtain g-C₃N₄/AgBr composites, wherein highly-dispersed AgBr having

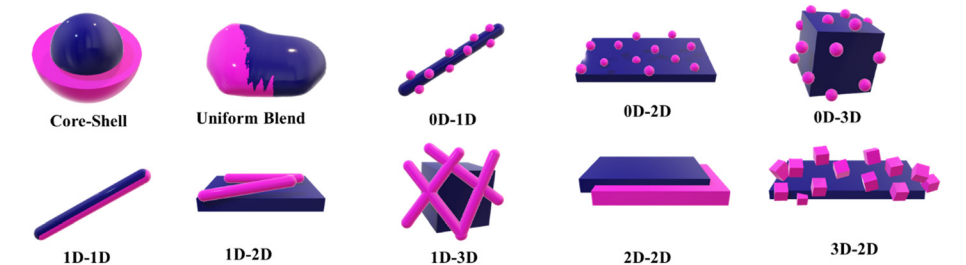


Fig. 6 A schematic depiction of various heterojunction structures based on morphology.

a size of ~1 nm in the g-C₃N₄ matrix exhibited efficient photocatalytic disinfection characteristics under both dark and light conditions.²⁹⁰ The high dispersion of the AgBr was

attributed to the surfactant-based precursor that dramatically reduced the interfacial tension during the process. In another study, g-C₃N₄/Ag₂S nanocomposites were synthesized by

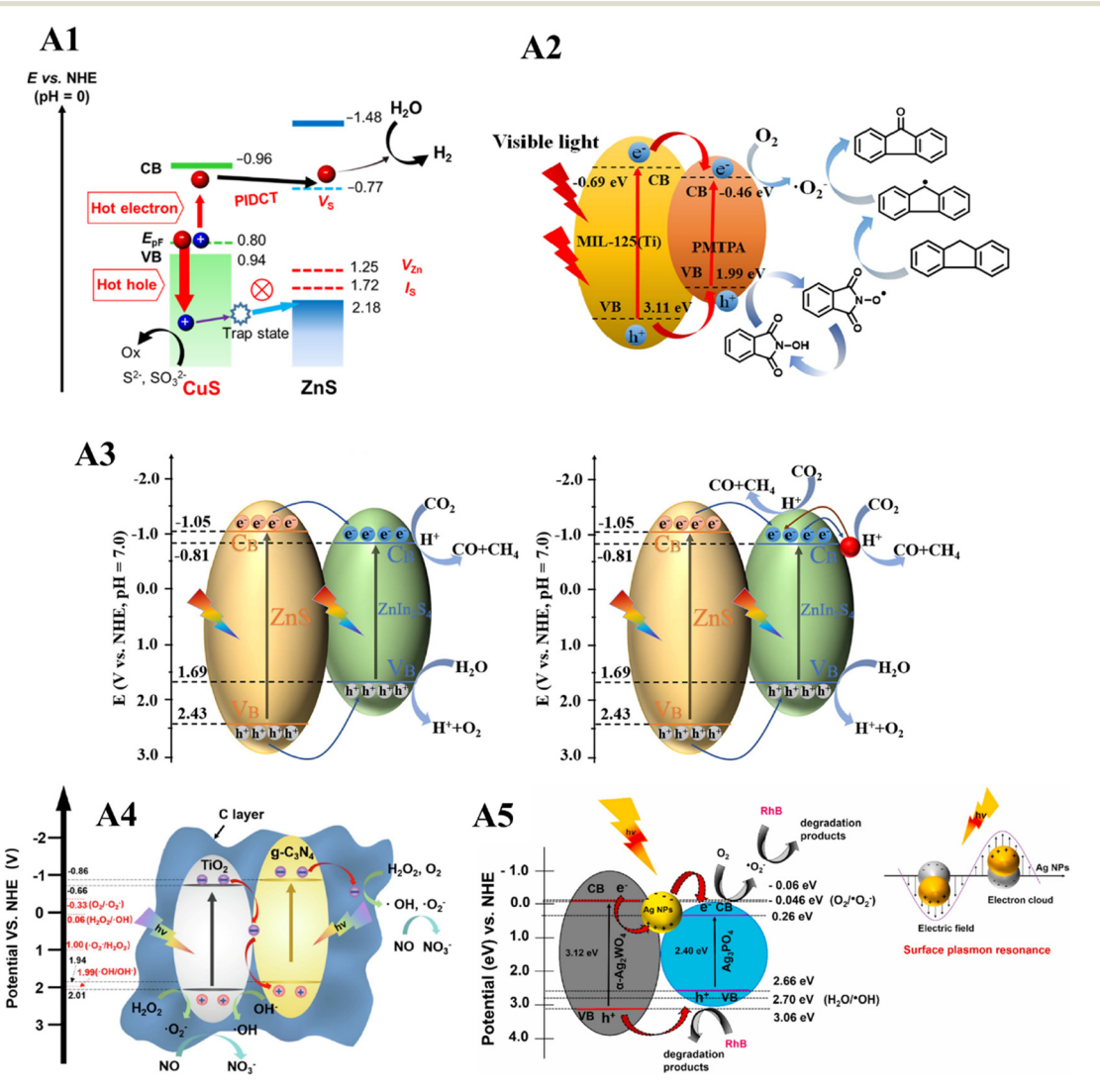


Fig. 7 Various applications of heterojunction catalysts. Plasmon-induced defect-mediated carrier transfer in CuS@ZnS core@shell nanocrystals for IR light responsive photocatalytic reaction (A1). Reproduced with permission from ref. 145. Copyright 2023 American Chemical Society. Fluorene photo-oxidation over MP-30 and N-hydroxyphthalimide (NHPI) (A2). Reproduced with permission from ref. 91. Copyright 2021 Elsevier B.V. CO₂ $photoreduction \ over \ 3-ZnS@ZnIn_2S_4 \ core-shell \ cages \ (left), \ and \ 3-ZnS@ZnIn_2S_4/Au \ core-shell \ cages \ (right) \ (A3). \ Reproduced \ with \ permission \ from \ Produced \ with \ permission \$ ref. 51. Copyright 2021 Elsevier Inc. Activation of hydrogen peroxide for NO removal over Z-scheme heterojunction catalyst TiO₂@C/g-C₃N₄ (A4). Reproduced with permission from ref. 120. Copyright 2021 Elsevier B.V. RhB degradation using developed heterojunction catalyst α-Ag₂WO₄/Ag₃-PO₄ (A5). Reproduced with permission from ref. 83. Copyright 2022 Elsevier B.V.

physically mixing melamine and silver amyl xanthate (Ag₂S precursor) and subjecting the resultant mixture to a one-step calcination process.²⁹¹ In this method, a significantly lower loading of Ag₂S than the theoretical estimate was observed, a factor that was attributed to the sublimation tendency of the sulphide. As a result, a two-step method was also explored, in which the Ag₂S precursor was physically mixed thoroughly over a pre-formed g-C₃N₄, which was then subjected to calcination. The nanocomposites obtained through the twostep method were found to result in an effective heterojunction that was proven by the enhancement in the density of states and minimization of the electron-hole recombination. These nanocomposites exhibited remarkable bactericidal efficacy under dark and visible light irradiation conditions.

Our group also fabricated a core-shell architecture via a solid-state synthesis, in which melamine was physically mixed with a pre-formed ZnO core.314 The thermolysis of the obtained blend resulted in the formation of a nitrogendeficient g-C₃N₄ shell, which formed an effective heterojunction with the ZnO core and was found to be responsible for the higher photocatalytic activity. In another study, by employing a customized sol-gel synthesis, we reported the formation of a heterojunction between the three polymorphs of TiO₂, namely, anatase, rutile, and brookite.³¹⁵ All three polymorphs and the phase composition were controlled through the thermal pretreatment of the gel. The enhancement in the photocatalytic activity of the triphasic TiO₂ was attributed to the effective heterojunction between the three polymorphs. Francis et al. reported the formation of the MOF-derived CuO/AgX (X = Cl, Br, I) nanocomposite to obtain a type I heterojunction. Calcination of silver halideloaded Cu-BTC MOF was found to yield intimately mixed CuO/AgX nanocomposites, which showed high photocatalytic activity attributed to the effective type-I heterojunction formed.316

Applications of heterojunction catalysis

Advancements in heterojunction catalysis allow for the precise tuning of catalyst characteristics, such as surface area, adsorption, functionalization, light absorption in UV, IR, or visible regions, and exciton redox potential, to suit various applications. Heterojunction catalysts have proven effective in diverse applications, including dye degradation, CO₂ reduction, NO_x manipulation, organic transformation 7).317,318 hydrogen generation (Fig. Organic transformation over heterojunction photocatalysis is also a promising avenue, considering the generation of waste to value-added products.³¹⁹

Tables 1-4 provide a comprehensive list of applications, including the type of heterojunction used, kinetic data of the reaction and other relevant reaction parameters employed.

Conclusions and future outlook

The field of heterojunction photocatalysis has evolved with the advent of various spectroscopic techniques and recent advances in simulations, which have facilitated the understanding of the plausible charge mechanism(s) between the coupled semiconductors. As a result, several effective heterojunctions have been developed for various applications such as organic pollutant abatement, water splitting, organic transformations, and CO₂ & NO_x reduction.

Following are a few excerpts from the various types of heterojunctions based on the charge transfer mechanisms mentioned in the review.

Type I: Enhances the charge separation, and the charge density is greater in the component with a narrow band gap, compromising with the redox potential.

Type II: Enhances the charge separation and light absorption with a near-uniform distribution of charges in both components, but compromises with the redox potential.

Z-scheme: Enhances the separation efficiency, improving light absorption and maintaining strong redox ability. However, the recombination of charges from the overall higher CB and lower VB is not completely averted.

S-scheme: Enhances the separation efficiency and light absorption while maintaining the high redox capability of the electrons and holes and providing an electric field at the interface for the recombination of charges with lower redox potential.

Type III: No/inefficient charge separation owing to broken gap band positions, which can be circumvented efficiently by adding a conducting component as the source of the hot charge transfer, i.e., converting to a type B heterojunction.

Looking to the future, a few prominent challenges and opportunities are listed below:

- (i) One of the major challenges faced in photocatalysis is deciphering the complex charge transfer mechanism. The mechanisms in many of the existing material compositions are not conclusive enough, which is otherwise significant, as some heterojunction categories vary marginally.
- (ii) The current trend shows a diversity in the material selection, which is expected to bring out much more efficient photocatalytic heterojunction compositions by making complex architectures like ternary and multicomponent systems.
- (iii) Within a given material composition, the synthetic methodology plays a vital role in deciding the performance. Hence, efficient synthetic strategies that result in tight heterojunction formation to facilitate a high degree of charge separation are required.
- (iv) Several opportunities exist in developing various material compositions and synthetic strategies that possess cumulative non-toxic, cost-effective, scalable, and industrially adaptable characteristics.

Conflicts of interest

The authors declare no competing interests.

References

- 1 A. K. Atri, S. Singh, I. Qadir, S. Sharma, U. Manhas and D. Singh, New J. Chem., 2023, 47, 12955-12972.
- 2 M. Qiu, W. Xu, S. Chen, Z. Jia, Y. Li, J. He, L. Wang, J. Lei, C. Liu and J. Liu, J. Taiwan Inst. Chem. Eng., 2023, 143, 104674.
- 3 A. Sheikhzadeh Takabi and A. Mouradzadegun, Photochem. Photobiol. Sci., 2023, 22, 837-855.
- 4 B. T. Son, N. V. Long and N. T. N. Hang, RSC Adv., 2021, 11, 30805-30826.
- 5 P. V. Kamat, ACS Energy Lett., 2018, 3, 1394-1395.
- 6 H. D. Muller and F. Steinbach, *Nature*, 1970, 225, 728-729.
- 7 A. Fujishima and K. Honda, Nature, 1972, 238, 37-38.
- 8 J. Schneider, M. Matsuoka, M. Takeuchi, J. Zhang, Y. Horiuchi, M. Anpo and D. W. Bahnemann, Chem. Rev., 2014, 114, 9919-9986.
- 9 M. H. Barzegar, M. M. Sabzehmeidani, M. Ghaedi, V. M. Avargani, Z. Moradi, V. A. L. Roy and H. Heidari, Chem. Eng. Res. Des., 2021, 174, 307-318.
- 10 E. Dupont, R. Koppelaar and H. Jeanmart, Appl. Energy, 2020, 257, 113968.
- 11 N. Serpone, E. Borgarello and M. Grätzel, J. Chem. Soc., Chem. Commun., 1984, 342-344.
- 12 I. Bedja and P. V. Kamat, J. Phys. Chem., 2002, 99, 9182-9188.
- 13 S. Ozkar, Dalton Trans., 2021, 50, 12349-12364.
- 14 J. Wang, Y. Yu, W. Xu, H. Yu, W. Zhang, H. Huang, G. R. Zhang and D. Mei, J. Catal., 2022, 411, 72-83.
- 15 C. Yuksel Alpaydın, S. K. Gulbay and C. Ozgur Colpan, Int. J. Hydrogen Energy, 2020, 45, 3414-3434.
- 16 D. Patra, R. Ganesan and B. Gopalan, Int. J. Hydrogen Energy, 2021, 46, 25486-25499.
- 17 Z. Zhang and J. T. J. Yates, Chem. Rev., 2012, 112, 5520-5551.
- 18 L. Wang, H. Yin, S. Wang, J. Wang and S. Ai, Appl. Catal., B, 2022, 305, 121039.
- 19 M. Murugalakshmi, G. Mamba, S. A. Ansari, V. Muthuraj and T. I. T. Nkambule, Colloids Surf., A, 2022, 634, 127969.
- 20 J. Huang, P. Xue, S. Wang, S. Han, L. Lin, X. Chen and Z. Wang, J. Colloid Interface Sci., 2022, 606, 1509-1523.
- 21 M. Sun, F. Li, F. Zhao, T. Wu, T. Yan, B. Du and D. Li, J. Colloid Interface Sci., 2022, 606, 1261-1273.
- 22 Y. Zhu, J. Xu and M. Chen, Sep. Purif. Technol., 2022, 282, 120004.
- 23 K. Qin, Q. Zhao, H. Yu, X. Xia, J. Li, S. He, L. Wei and T. An, Environ. Res., 2021, 199, 111360.
- 24 K. Girija, S. Thirumalairajan, V. R. Mastelaro and D. Mangalaraj, J. Mater. Chem. A, 2015, 3, 2617-2627.
- 25 Y. Nosaka and A. Y. Nosaka, Chem. Rev., 2017, 117, 11302-11336.

- 26 W. J. Ong, L. L. Tan, Y. H. Ng, S. T. Yong and S. P. Chai, Chem. Rev., 2016, 116, 7159-7329.
- 27 A. Wadsworth, Z. Hamid, J. Kosco, N. Gasparini and I. McCulloch, Adv. Mater., 2020, 32, 2001763.
- 28 H. Yang, Mater. Res. Bull., 2021, 142, 111406.
- 29 Z. Xiong, O. Liu, Z. Gao, J. Yang, X. Zhang, O. Yang and C. Hao, Inorg. Chem., 2021, 60, 5063-5070.
- 30 P. Kumari, N. Bahadur, L. Kong, L. A. O'Dell, A. Merenda and L. Dumee, Mater. Adv., 2022, 2309-2323.
- 31 H. Wang, L. Zhang, Z. Chen, J. Hu, S. Li, Z. Wang, J. and X. Wang, Chem. Soc. Rev., 2014, 43, 5234-5244.
- 32 H. Zhao, X. Liu, Y. Dong, Y. Xia, H. Wang and X. Zhu, ACS Appl. Mater. Interfaces, 2020, 12, 31532-31541.
- 33 A. Wang, S. Wu, J. Dong, R. Wang, J. Wang, J. Zhang, S. Zhong and S. Bai, Chem. Eng. J., 2021, 404, 127145.
- 34 S. Lu, B. Weng, A. Chen, X. Li, H. Huang, X. Sun, W. Feng, Y. Lei, Q. Qian and M.-Q. Yang, ACS Appl. Mater. Interfaces, 2021, 13, 13044-13054.
- 35 Z. Li, W. Huang, J. Liu, K. Lv and Q. Li, ACS Catal., 2021, 11, 8510-8520.
- 36 Z. Liang, B. Ouyang, T. Wang, X. Liu, H. Huo, D. Liu, H. Feng, J. Ma, K. Deng, A. Li and others, Int. J. Hydrogen Energy, 2022, 47, 10868-10876.
- 37 C. Li, G. Ding, X. Liu, P. Huo, Y. Yan, Y. Yan and G. Liao, Chem. Eng. J., 2022, 435, 134740.
- 38 N. Tian, H. Huang, S. Wang, T. Zhang, X. Du and Y. Zhang, Appl. Catal., B, 2020, 267, 118697.
- 39 K. S. Novoselov, A. K. Geim, S. V. Morozov, D. Jiang, Y. Zhang, S. V. Dubonos, I. V. Grigorieva and A. A. Firsov, Science, 2004, 306, 666-669.
- 40 X. Chen, W. Pan, R. Guo, X. Hu, Z. Bi and J. Wang, J. Mater. Chem. A, 2022, 10, 7604-7625.
- 41 W. Jia, B. Ding, X. Qian, Y. Yang, L. Mao, X. Cai, S. Guo and J. Zhang, J. Phys. Chem. C, 2021, 125, 19763-19772.
- 42 Y. Zhou, C. Zhang, D. Huang, W. Wang, Y. Zhai, Q. Liang, Y. Yang, S. Tian, H. Luo and D. Qin, Appl. Catal., B, 2022, 301, 120749.
- 43 G. Yao, S. Yang, S. Jiang, C. Sun and S. Song, Appl. Catal., B, 2022, 121569.
- 44 Y. Xu, X. Jin, T. Ge, H. Xie, R. Sun, F. Su, X. Li and L. Ye, Chem. Eng. J., 2021, 409, 128178.
- 45 W. Hu and J. Yang, J. Mater. Chem. C, 2017, 5, 12289-12297.
- 46 S. Bao, Z. Wang, J. Zhang and B. Tian, ACS Appl. Nano Mater., 2020, 3, 8604-8617.
- 47 Y. Luo, G. Sun, B. Tian and J. Zhang, Chem. Eng. J., 2022, 442, 135835.
- 48 P. Gao, S. Huang, K. Tao, Z. Li, L. Feng, Y. Liu and L. Zhang, J. Hazard. Mater., 2022, 129374.
- 49 L. Zhang, Y. Meng, H. Shen, J. Li, C. Yang, B. Xie and S. Xia, Inorg. Chem., 2022, 61, 6045-6055.
- 50 J. Low, J. Yu, M. Jaroniec, S. Wageh and A. A. Al-Ghamdi, Adv. Mater., 2017, 29, 1601694.
- 51 Y. Zhao, Y. Chen, L. Du, Q. Wang, X. Liu, L. Li and G. Tian, J. Colloid Interface Sci., 2022, 605, 253-262.

- 52 S. Joshi, R. K. Canjeevaram Balasubramanyam, S. J. Ippolito, Y. M. Sabri, A. E. Kandjani, S. K. Bhargava and M. V. Sunkara, ACS Appl. Nano Mater., 2018, 1, 3375-3388.
- 53 S. Challagulla, R. Nagarjuna, R. Ganesan and S. Roy, ACS Sustainable Chem. Eng., 2016, 4, 974-982.
- 54 L. Zhang, X. Dong, Y. Wang, N. Zheng, H. Ma and X. Zhang, Appl. Surf. Sci., 2022, 579, 152088.
- 55 X. Liu, Y. Liu, T. Liu, Y. Jia, H. Deng, W. Wang and F. Zhang, Chem. Eng. J., 2022, 431, 134181.
- 56 C. Li, H. Sun, H. Jin, W. Li, J. L. Liu and S. Bashir, Catal. Today, 2022, 400, 146-158.
- 57 Q. Xu, L. Zhang, B. Cheng, J. Fan and J. Yu, Chem, 2020, 6, 1543-1559.
- 58 A. J. Bard, J. Photochem., 1979, 10, 59-75.
- 59 J. Low, C. Jiang, B. Cheng, S. Wageh, A. A. Al-Ghamdi and J. Yu, Small Methods, 2017, 1, 1700080.
- 60 Q. Xu, L. Zhang, J. Yu, S. Wageh, A. A. Al-Ghamdi and M. Jaroniec, Mater. Today, 2018, 21, 1042-1063.
- 61 K. Maeda, ACS Catal., 2013, 3, 1486-1503.
- 62 X. Li, C. Garlisi, Q. Guan, S. Anwer, K. Al-Ali, G. Palmisano and L. Zheng, Mater. Today, 2021, 47, 75-107.
- 63 C. Xing, G. Yu, J. Zhou, Q. Liu, T. Chen, H. Liu and X. Li, Appl. Catal., B, 2022, 121496.
- 64 W. Zhang, A. R. Mohamed and W.-J. Ong, Angew. Chem., Int. Ed., 2020, **59**, 22894–22915.
- 65 P. Zhou, J. Yu and M. Jaroniec, Adv. Mater., 2014, 26, 4920-4935.
- 66 T. Di, Q. Xu, W. Ho, H. Tang, Q. Xiang and J. Yu, ChemCatChem, 2019, 11, 1394-1411.
- 67 B. J. Ng, L. K. Putri, X. Y. Kong, Y. W. Teh, P. Pasbakhsh and S. P. Chai, Adv. Sci., 2020, 7, 1903171.
- 68 Y. Xue, W. Tang, C. Si, Q. Lu, E. Guo, M. Wei and Y. Pang, Opt. Mater., 2022, 128, 112400.
- 69 S. Pu, Y. Chen, D. Wang, Y. Zhang, Y. Li, W. Feng and Y. Sun, Opt. Mater., 2023, 141, 113888.
- 70 M. He, J. Chen, Y. Yang, X. Hu, Z. Jiang, Y. Yan, J. Sun, L. Fu, J. Wei and T. Yang, Opt. Mater., 2023, 137, 113554.
- 71 Y. Wang, S. Feng, C. Ma, Y. Zhou, Z. Ye, X. Dai and X. Cao, Opt. Mater., 2023, 135, 113087.
- 72 J. Fu, Q. Xu, J. Low, C. Jiang and J. Yu, Appl. Catal., B, 2019, 243, 556-565.
- 73 P. Xia, S. Cao, B. Zhu, M. Liu, M. Shi, J. Yu and Y. Zhang, Angew. Chem., Int. Ed., 2020, 59, 5218-5225.
- 74 S. Li, C. Wang, M. Cai, F. Yang, Y. Liu, J. Chen, P. Zhang, X. Li and X. Chen, Chem. Eng. J., 2022, 428, 131158.
- 75 F. Xu, K. Meng, B. Cheng, S. Wang, J. Xu and J. Yu, Nat. Commun., 2020, 11, 1-9.
- 76 C. Cheng, B. He, J. Fan, B. Cheng, S. Cao and J. Yu, Adv. Mater., 2021, 33, 2100317.
- 77 S. J. A. Moniz, S. A. Shevlin, D. J. Martin, Z. X. Guo and J. Tang, Energy Environ. Sci., 2015, 8, 731-759.
- 78 J. Li, X. Yang, C. Ma, Y. Lei, Z. Cheng and Z. Rui, Appl. Catal., B, 2021, 291, 120053.
- 79 J. Li, J. Chen, H. Fang, X. Guo and Z. Rui, Ind. Eng. Chem. Res., 2021, 60, 8420-8429.

- 80 J. Li, J. Feng, X. Guo, H. Fang, J. Chen, C. Ma, R. Li, Y. Wang and Z. Rui, Appl. Catal., B, 2022, 309, 121248.
- 81 A. D. Lopis, K. S. Choudhari, R. Sai, K. S. Kanakikodi, S. P. Maradur, S. A. Shivashankar and S. D. Kulkarni, Sol. Energy, 2022, 240, 57-68.
- 82 O. Mao, D. Li and Y. Dong, New J. Chem., 2022, 46, 6267-6273.
- 83 A. B. Trench, R. Alvarez, V. Teodoro, L. G. da Trindade, T. R. Machado, M. M. Teixeira, D. de Souza, I. M. Pinatti, A. Z. Simões, Y. G. Gobato and others, Mater. Chem. Phys., 2022, 280, 125710.
- 84 J. Li, Y. Mei, S. Ma, Q. Yang, B. Jiang, B. Xin, T. Yao and J. Wu, J. Colloid Interface Sci., 2022, 608, 2075-2087.
- 85 X. Ji, R. Guo, J. Tang, Z. Lin, Y. Yuan, L. Hong and W. Pan, J. Colloid Interface Sci., 2022, 618, 300-310.
- 86 L. Zhang, Z. Q. Wang, J. Liao, X. Zhang, D. Feng, H. Deng and C. Ge, Chem. Eng. J., 2022, 431, 133453.
- 87 C. Liu, J. Xu, X. Du, Q. Li, Y. Fu and M. Chen, Opt. Mater., 2021, 112, 110742.
- 88 S. Q. Guo, H. Zhang, Z. Hu, M. Zhen, B. Yang, B. Shen and F. Dong, Nano Res., 2021, 14, 4188-4196.
- 89 W. Guo, J. Li, Y. Yang, M. Zhang, Y. Zhai, D. Li, H. Zhao and Y. Liu, Mater. Chem. Phys., 2021, 264, 124440.
- 90 S. A. Younis, E. Amdeha and R. A. El-Salamony, J. Environ. Chem. Eng., 2021, 9, 104619.
- 91 Z. Wu, K. Zhang, X. Li, G. Hai, X. Huang and G. Wang, Appl. Surf. Sci., 2021, 555, 149732.
- 92 H. He, W. Wang, C. Xu, S. Yang, C. Sun, X. Wang, Y. Yao, N. Mi, W. Xiang, S. Li and others, Sci. Total Environ., 2020, 730, 139100.
- 93 M. Xiong, J. Yan, B. Chai, G. Fan and G. Song, J. Mater. Sci. Technol., 2020, 56, 179-188.
- 94 Y. Li, X. Wang, H. Huo, Z. Li and J. Shi, Colloids Surf., A, 2020, 587, 124322.
- 95 R. Li, X. Li, J. Wu, X. Lv, Y. Z. Zheng, Z. Zhao, X. Ding, X. Tao and J. F. Chen, *Appl. Catal.*, *B*, 2019, **259**, 118075.
- 96 M. Nikookar, A. Rezaeifard, K. V. Grzhegorzhevskii, M. Jafarpour and R. Khani, ACS Appl. Nano Mater., 2022, 7917-7931.
- 97 M. Li, Y. Wang, N. Tian and H. Huang, Appl. Surf. Sci., 2022, 587, 152852.
- 98 U. Kumar, J. Kuntail, A. Kumar, R. Prakash, M. R. Pai and I. Sinha, Appl. Surf. Sci., 2022, 589, 153013.
- 99 E. Alimohammadi, V. Mahdikhah and S. Sheibani, Appl. Surf. Sci., 2022, 598, 153816.
- 100 J. Wang, B. Wang, W. Zhang, Y. Xiao, H. Xu, Y. Liu, Z. Liu, J. Zhang and Y. Jiang, Appl. Surf. Sci., 2022, 587, 152867.
- 101 Q. Dong, Z. Chen, B. Zhao, Y. Zhang, Z. Lu, X. Wang, J. Li and W. Chen, J. Colloid Interface Sci., 2022, 608, 1951-1959.
- 102 X. Li, J. Wang, J. Zhang, C. Zhao, Y. Wu and Y. He, J. Colloid Interface Sci., 2022, 607, 412-422.
- 103 X. Zhang, X. Yang, B. Liu, G. Zhu and J. Fan, J. Environ. Chem. Eng., 2022, 10, 107068.
- 104 X. Wu, J. Lu, S. Huang, X. Shen, S. Cui and X. Chen, Appl. Surf. Sci., 2022, 594, 153486.

- 105 Y. He, J. Shi, Q. Yang, Y. Tong, Z. Ma, L. B. Junior and B. Yao, Chem. Eng. J., 2022, 137355.
- 106 L. Sun, W. Wang, C. Zhang, M. Cheng, Y. Zhou, Y. Yang, H. Luo, D. Qin, C. Huang and Z. Ouyang, Chem. Eng. J., 2022, 137027.
- 107 Y. R. Lv, Z. L. Wang, Y. X. Yang, Y. Luo, S. Y. Yang and Y. H. Xu, J. Hazard. Mater., 2022, 432, 128665.
- 108 J. Yang, Y. Wu, Y. Dong, H. Cui, C. Shi, H. Sun and S. Yin, J. Ind. Eng. Chem., 2022, 509-518.
- 109 F. Chen, K. Bian, H. Li, Y. Tang, C. Hao and W. Shi, J. Chem. Technol. Biotechnol., 2022, 97, 1884-1892.
- 110 T. Kulandaivalu, A. R. Mohamed, K. A. Ali and S. Kulandaivalu, J. CO2 Util., 2022, 63, 102115.
- 111 C. Jing, Y. Zhang, J. Zheng, S. Ge, J. Lin, D. Pan, N. Naik and Z. Guo, Particuology, 2022, 69, 111-122.
- 112 G. Kumar, J. Kumar, M. Bag and R. K. Dutta, Sep. Purif. Technol., 2022, 292, 121040.
- 113 V. Poliukhova, S. Khan, Z. Qiaohong, J. Zhang, D. Kim, S. Kim and S. H. Cho, Appl. Surf. Sci., 2022, 575, 151773.
- 114 J. Li, H. Liu, Z. Liu, D. Yang, M. Zhang, L. Gao, Y. Zhou and C. Lu, Arabian J. Chem., 2022, 15, 103513.
- 115 C. Lan, L. Meng and N. Xu, Colloids Surf., A, 2022, 632, 127762.
- 116 J. Yang, C. Shi, Y. Dong, H. Su, H. Sun, Y. Guo and S. Yin, J. Colloid Interface Sci., 2022, 605, 373-384.
- 117 S. Dhingra, M. Sharma, V. Krishnan and C. M. Nagaraja, J. Colloid Interface Sci., 2022, 608, 1040-1050.
- 118 Z. Huang, J. Liu, S. Zong, X. Wang, K. Chen, L. Liu and Y. Fang, J. Colloid Interface Sci., 2022, 606, 848-859.
- 119 K. Ouyang, B. Xu, C. Yang, H. Wang, P. Zhan and S. Xie, Mater. Sci. Semicond. Process., 2022, 137, 106168.
- 120 T. Wang, W. Yang, L. Chang, H. Wang, H. Wu, J. Cao, H. Fan, J. Wang, H. Liu, Y. Hou and others, Sep. Purif. Technol., 2022, 285, 120329.
- 121 Z. Hu, D. Shi, G. Wang, T. Gao, J. Wang, L. Lu and J. Li, Appl. Surf. Sci., 2022, 154167.
- 122 J. Li, F. Wei, Z. Xiu and X. Han, Chem. Eng. J., 2022, 137129.
- 123 H. Yu, Y. Xue, S. Liang and X. Wang, J. Photochem. Photobiol., A, 2022, 114077.
- 124 C. Wu, Q. Shen, J. Liu, L. Jiang, J. Sheng, Y. Li and H. Yang, J. Photochem. Photobiol., A, 2022, 114142.
- 125 R. Guo, Z. Bi, Z. Lin, X. Hu, J. Wang, X. Chen and W. Pan, J. Colloid Interface Sci., 2022, 627, 343-354.
- 126 J. Yao, L. Huang, Y. Li, J. Liu, J. Liu, S. Shu, L. Huang and Z. Zhang, J. Colloid Interface Sci., 2022, 627, 224–237.
- 127 Y. Wang, Y. Liu, F. Tian, S. Bao, C. Sun, W. Yang and Y. Yu, J. Colloid Interface Sci., 2022, 264-277.
- 128 N. Lu, X. Jing, J. Zhang, P. Zhang, Q. Qiao and Z. Zhang, Chem. Eng. J., 2022, 431, 134001.
- 129 Y. Su, X. Xu, R. Li, X. Luo, H. Yao, S. Fang, K. P. Homewood, Z. Huang, Y. Gao and X. Chen, Chem. Eng. J., 2022, 429, 132241.
- 130 Z. Jin, X. Jiang and X. Guo, Int. J. Hydrogen Energy, 2022, 47, 1669-1682.
- 131 S. Xiao, Y. Guan, H. Shang, H. Li, Z. Tian, S. Liu, W. Chen and J. Yang, J. CO2 Util., 2022, 55, 101806.

- 132 X. Xu, Y. Su, Y. Dong, X. Luo, S. Wang, W. Zhou, R. Li, K. P. Homewood, X. Xia, Y. Gao and others, J. Hazard. Mater., 2022, 424, 127685.
- 133 Z. Zhang, M. Wang, Z. Chi, W. Li, H. Yu, N. Yang and H. Yu, Appl. Catal., B, 2022, 313, 121426.
- 134 X. Han, B. Lu, X. Huang, C. Liu, S. Chen, J. Chen, Z. Zeng, S. Deng and J. Wang, Appl. Catal., B, 2022, 121587.
- 135 L. Chen, X. L. Song, J. T. Ren and Z. Y. Yuan, Appl. Catal., B, 2022, 315, 121546.
- 136 F. A. Qaraah, S. A. Mahyoub, A. Hezam, A. Qaraah, F. Xin and G. Xiu, Appl. Catal., B, 2022, 121585.
- 137 K. Wang, X. Shao, K. Zhang, J. Wang, X. Wu and H. Wang, Appl. Surf. Sci., 2022, 596, 153444.
- 138 J. Bai, W. Chen, L. Hao, R. Shen, P. Zhang, N. Li and X. Li, Chem. Eng. J., 2022, 447, 137488.
- 139 J. Zheng, C. Fan, X. Li, Q. Yang, D. Wang, A. Duan, J. Ding, S. Rong, Z. Chen, J. Luo and others, Chem. Eng. J., 2022, 137371.
- 140 C. Wang, H. Liu, G. Wang, H. Fang, X. Yuan and C. Lu, Chem. Eng. J., 2022, 450, 138167.
- 141 B. Zhang, D. Wang, S. Jiao, Z. Xu, Y. Liu, C. Zhao, J. Pan, D. Liu, G. Liu, B. Jiang and others, Chem. Eng. J., 2022, 137138.
- 142 Y. Zhang, J. Qiu, B. Zhu, M. V. Fedin, B. Cheng, J. Yu and L. Zhang, Chem. Eng. J., 2022, 444, 136584.
- 143 D. D. Blach, W. Zheng, H. Liu, A. Pan and L. Huang, J. Phys. Chem. C, 2020, 124, 11325-11332.
- 144 A. Iqbal, A. Kafizas, C. Sotelo-Vazquez, R. Wilson, M. Ling, A. Taylor, C. Blackman, K. Bevan, I. Parkin and R. Quesada-Cabrera, ACS Appl. Mater. Interfaces, 2021, 13, 9781-9793.
- 145 Z. Lian, F. Wu, J. Zi, G. Li, W. Wang and H. Li, J. Am. Chem. Soc., 2023, 145, 15482-15487.
- 146 W. Wang, Y. Tao, J. Fan, Z. Yan, H. Shang, D. L. Phillips, M. Chen and G. Li, Adv. Funct. Mater., 2022, 32, 2201357.
- 147 G. N. Schrauzer and T. D. Guth, J. Am. Chem. Soc., 1977, 99, 7189-7193.
- 148 R. Nagarjuna, S. Roy and R. Ganesan, Microporous Mesoporous Mater., 2015, 211, 1-8.
- 149 R. Nagarjuna, S. Challagulla, N. Alla, R. Ganesan and S. Roy, Mater. Des., 2015, 86, 621-626.
- 150 S. Challagulla, K. Tarafder, R. Ganesan and S. Roy, J. Phys. Chem. C, 2017, 121, 27406-27416.
- 151 S. Challagulla, K. Tarafder, R. Ganesan and S. Roy, Sci. Rep., 2017, 7, 1-11.
- 152 J. Wu, Y. Tao, C. Zhang, Q. Zhu, D. Zhang and G. Li, J. Hazard. Mater., 2023, 443, 130363.
- 153 Evonik, AEROXIDE, AERODISP and AEROPERL, Titanium Dioxide as Photocatalyst, Technical Information 1243, Evonik Industries, 2015, pp. 4-11.
- 154 A. M. Pennington, A. I. Okonmah, D. T. Munoz, G. Tsilomelekis and F. E. Celik, J. Phys. Chem. C, 2018, 122, 5093-5104.
- 155 D. Zhang, Z. Liu and R. Mou, Inorg. Chem. Commun., 2022, 109667.
- 156 V. Dutta, S. Sharma, P. Raizada, V. K. Thakur, A. A. P. Khan, V. Saini, A. M. Asiri and P. Singh, J. Environ. Chem. Eng., 2021, 9, 105018.

- 157 S. Ali, A. Razzaq, H. Kim and S. I. In, Chem. Eng. J., 2022, 429, 131579.
- 158 A. H. Zahid and Q. Han, Nanoscale, 2021, 17687-17724.
- 159 A. Ghenaatgar, R. M. A. Tehrani and A. Khadir, J. Water Process Eng., 2019, 32, 100969.
- 160 R. Nagarjuna, S. Challagulla, R. Ganesan and S. Roy, Chem. Eng. J., 2017, 308, 59-66.
- 161 R. Nagarjuna, S. Challagulla, P. Sahu, S. Roy and R. Ganesan, Adv. Powder Technol., 2017, 28, 3265-3273.
- 162 M. Galedari, M. M. Ghazi and S. R. Mirmasoomi, Chem. Eng. Res. Des., 2021, 170, 248-255.
- 163 P. H. Palharim, M. C. D. Caira, C. de Araujo Gusmao, B. Ramos, G. T. dos Santos, O. Rodrigues Jr and A. C. S. C. Teixeira, Chem. Eng. Res. Des., 2022, 188, 935-953.
- 164 K. Kannan, D. Radhika, K. K. Sadasivuni, K. R. Reddy and A. V. Raghu, Adv. Colloid Interface Sci., 2020, 281, 102178.
- 165 L. Chen, Z. Liu, Z. Guo and X. J. Huang, J. Mater. Chem. A, 2020, 8, 17326-17359.
- 166 H. Mai, D. Chen, Y. Tachibana, H. Suzuki, R. Abe and R. A. Caruso, Chem. Soc. Rev., 2021, 50, 13692-13729.
- 167 K. Wei, Y. Faraj, G. Yao, R. Xie and B. Lai, Chem. Eng. J., 2021, 414, 128783.
- 168 O. B. Olgun, B. Palas, S. Atalay and G. Ersoz, Chem. Eng. Res. Des., 2021, 171, 421-432.
- 169 K. S. Schanze, P. V. Kamat, P. Yang and J. Bisquert, ACS Energy Lett., 2020, 8, 2602-2604.
- 170 J. Wang, J. Liu, Z. Du and Z. Li, J. Energy Chem., 2021, 54, 770-785.
- 171 A. Rahman and M. M. Khan, New J. Chem., 2021, 19622-19635.
- 172 R. Woods-Robinson, Y. Han, H. Zhang, T. Ablekim, I. Khan, K. A. Persson and A. Zakutayev, Chem. Rev., 2020, 120, 4007-4055.
- 173 K. Muralirajan, R. Kancherla, J. A. Bau, M. R. Taksande, M. Qureshi, K. Takanabe and M. Rueping, ACS Catal., 2021, 11, 14772-14780.
- 174 Y. Bai, Q. Zhang, N. Xu, K. Deng and E. Kan, Appl. Surf. Sci., 2019, 478, 522-531.
- 175 M. M. Chen, H. G. Xue and S. P. Guo, Coord. Chem. Rev., 2018, 368, 115-133.
- 176 E. Wlazlak, A. Blachecki, M. Bisztyga-Szklarz, S. Klejna, T. Mazur, K. Mech, K. Pilarczyk, D. Przyczyna, M. Suchecki, P. Zawal and others, Chem. Commun., 2018, 54, 12133-12162.
- 177 G. Cai, P. Yan, L. Zhang, H. C. Zhou and H. L. Jiang, Chem. Rev., 2021, 121, 12278-12326.
- 178 M. Ahmed, Inorg. Chem. Front., 2022, 3003-3033.
- 179 K. Geng, T. He, R. Liu, S. Dalapati, K. T. Tan, Z. Li, S. Tao, Y. Gong, Q. Jiang and D. Jiang, Chem. Rev., 2020, 120, 8814-8933.
- 180 Z. Wang, J. Huang, J. Mao, Q. Guo, Z. Chen and Y. Lai, J. Mater. Chem. A, 2020, 8, 2934-2961.
- 181 G. Zhang, D. Huang, M. Cheng, L. Lei, S. Chen, R. Wang, W. Xue, Y. Liu, Y. Chen and Z. Li, J. Mater. Chem. A, 2020, 8, 17883-17906.
- 182 Q. Wang, Q. Gao, A. M. Al-Enizi, A. Nafady and S. Ma, *Inorg.* Chem. Front., 2020, 7, 300-339.

- 183 J. Meng, X. Liu, C. Niu, Q. Pang, J. Li, F. Liu, Z. Liu and L. Mai, Chem. Soc. Rev., 2020, 49, 3142-3186.
- 184 C. Du, Z. Zhang, G. Yu, H. Wu, H. Chen, L. Zhou, Y. Zhang, Y. Su, S. Tan, L. Yang, J. Song and S. Wang, Chemosphere, 2021, 272, 129501.
- 185 O. Guan, L. L. Zhou and Y. B. Dong, Chem. Soc. Rev., 2022, 6307-6416.
- 186 Z. He, J. Goulas, E. Parker, Y. Sun, X. Zhou and L. Fei, Catal. Today, 2023, 409, 103-118.
- 187 J. Li, D. Zhao, J. Liu, A. Liu and D. Ma, Molecules, 2020, 25, 2425.
- 188 R. Liu, K. T. Tan, Y. Gong, Y. Chen, Z. Li, S. Xie, T. He, Z. Lu, H. Yang and D. Jiang, Chem. Soc. Rev., 2021, 50, 120-242.
- 189 C. Xia, K. O. Kirlikovali, T. H. C. Nguyen, X. C. Nguyen, Q. B. Tran, M. K. Duong, M. T. N. Dinh, D. L. T. Nguyen, P. Singh, P. Raizada and others, Coord. Chem. Rev., 2021, 446, 214117.
- 190 J. You, Y. Zhao, L. Wang and W. Bao, J. Cleaner Prod., 2021, 291, 125822.
- 191 D. G. Wang, T. Qiu, W. Guo, Z. Liang, H. Tabassum, D. Xia and R. Zou, Energy Environ. Sci., 2021, 14, 688-728.
- 192 N. Keller and T. Bein, Chem. Soc. Rev., 2021, 50, 1813-1845.
- 193 G. B. Wang, S. Li, C. X. Yan, F. C. Zhu, Q. Q. Lin, K. H. Xie, Y. Geng and Y.-B. Dong, J. Mater. Chem. A, 2020, 8,
- 194 H. Wang, H. Wang, Z. Wang, L. Tang, G. Zeng, P. Xu, M. Chen, T. Xiong, C. Zhou, X. Li and others, Chem. Soc. Rev., 2020, 49, 4135-4165.
- 195 Q. Yang, M. Luo, K. Liu, H. Cao and H. Yan, Appl. Catal., B, 2020, 276, 119174.
- 196 T. Banerjee, K. Gottschling, G. Savasci, C. Ochsenfeld and B. V. Lotsch, ACS Energy Lett., 2018, 3, 400-409.
- 197 C. Guo, F. Duan, S. Zhang, L. He, M. Wang, J. Chen, J. Zhang, Q. Jia, Z. Zhang and M. Du, J. Mater. Chem. A, 2022, 10, 475-507.
- 198 S. Y. Hu, Y. N. Sun, Z. W. Feng, F. O. Wang and Y. Lv, Chemosphere, 2022, 286, 131646.
- 199 M. Naguib, M. Kurtoglu, V. Presser, J. Lu, J. Niu, M. Heon, L. Hultman, Y. Gogotsi and M. W. Barsoum, Adv. Mater., 2011, 23, 4248-4253.
- 200 A. A. Fadahunsi, C. Li, M. I. Khan and W. Ding, J. Mater. Chem. B, 2022, 4331-4345.
- 201 T. Su, X. Ma, J. Tong, H. Ji, Z. Z. Qin and Z. Wu, J. Mater. Chem. A, 2022, 10265-10296.
- 202 N. H. Solangi, R. R. Karri, S. A. Mazari, N. M. Mubarak, A. S. Jatoi, G. Malafaia and A. K. Azad, Coord. Chem. Rev., 2023, 477, 214965.
- 203 Z. You, Y. Liao, X. Li, J. Fan and Q. Xiang, Nanoscale, 2021, 13, 9463-9504.
- 204 J. Jin, T. Xiao, Y. Zhang, H. Zheng, H. Wang, R. Wang, Y. Gong, B. He, X. Liu and K. Zhou, Nanoscale, 2021, 13, 19740-19770.
- 205 S. Ponnada, M. S. Kiai, D. B. Gorle, R. Venkatachalam, B. Saini, K. Murugavel, A. Nowduri, R. Singhal, F. Marken,

- A. M. Kulandainathan and others, Catal. Sci. Technol., 2022, 4413-4441.
- 206 X. Chen, Z. Shi, Y. Tian, P. Lin, D. Wu, X. Li, B. Dong, W. Xu and X. Fang, Mater. Horiz., 2021, 8, 2929-2963.
- 207 J. Xu, T. Peng, X. Qin, Q. Zhang, T. Liu, W. Dai, B. Chen, H. Yu and S. Shi, J. Mater. Chem. A, 2021, 9, 14147-14171.
- 208 A. D. Handoko, S. N. Steinmann and Z. W. Seh, Nanoscale Horiz., 2019, 4, 809-827.
- 209 J. Pang, R. G. Mendes, A. Bachmatiuk, L. Zhao, H. Q. Ta, T. Gemming, H. Liu, Z. Liu and M. H. Rummeli, Chem. Soc. Rev., 2019, 48, 72-133.
- 210 F. Song, G. Li, Y. Zhu, Z. Wu, X. Xie and N. Zhang, J. Mater. Chem. A, 2020, 8, 18538-18559.
- 211 A. M. Alexander and J. S. J. Hargreaves, Chem. Soc. Rev., 2010, 39, 4388-4401.
- 212 Y. Zhang, Y. Hu, H. Zeng, L. Zhong, K. Liu, H. Cao, W. Li and H. Yan, J. Hazard. Mater., 2017, 329, 22-29.
- 213 B. Ma, D. Li, X. Wang and K. Lin, ChemSusChem, 2018, 11, 3871-3881.
- 214 G. Tuci, Y. Liu, A. Rossin, X. Guo, C. Pham, G. Giambastiani and C. Pham-Huu, Chem. Rev., 2021, 121, 10559-10665.
- 215 Y. Chen, H. Zhang, J. Zhang, J. Ma, L. Wang, H. Ye, G. Qian and Y. Ye, Adv. Powder Technol., 2013, 24, 207-211.
- 216 J. Liu, S. Wen, Y. Hou, F. Zuo, G. J. O. Beran and P. Feng, Angew. Chem., 2013, 125, 3323-3327.
- 217 A. T. Garcia-Esparza, D. Cha, Y. Ou, J. Kubota, K. Domen and K. Takanabe, ChemSusChem, 2013, 6, 168-181.
- 218 Y. Pan, T. Zhou, J. Han, J. Hong, Y. Wang, W. Zhang and R. Xu, Catal. Sci. Technol., 2016, 6, 2206-2213.
- 219 Y. X. Pan, H. Q. Zhuang, H. Ma, J. Cheng and J. Song, Chem. Eng. Sci., 2019, 194, 71-77.
- 220 Y. Lei, K. H. Ng, Y. Zhang, Z. Li, S. Xu, J. Huang and Y. Lai, Chem. Eng. J., 2022, 434, 134689.
- 221 B. P. Mabuea, H. C. Swart and E. Erasmus, ACS Omega, 2022, 7, 23401-23411.
- 222 Y. Zhang, T. Xia, P. Wallenmeyer, C. X. Harris, A. A. Peterson, G. A. Corsiglia, J. Murowchick and X. Chen, Energy Technol., 2014, 2, 183-187.
- 223 B. Wang, Y. Wang, Y. Lei, N. Wu, Y. Gou, C. Han, S. Xie and D. Fang, Nano Res., 2016, 9, 886-898.
- 224 J. Hong, S. S. Meysami, V. Babenko, C. Huang, S. Luanwuthi, J. Acapulco, P. Holdway, P. S. Grant and N. Grobert, Appl. Catal., B, 2017, 218, 267–276.
- 225 F. Chang, J. Zheng, X. Wang, Q. Xu, B. Deng, X. Hu and X. Liu, Mater. Sci. Semicond. Process., 2018, 75, 183-192.
- 226 O. Koysuren, J. Appl. Polym. Sci., 2020, 137, 48524.
- 227 H. Li and J. Sun, ACS Appl. Mater. Interfaces, 2021, 13, 5073-5078.
- 228 L. Tian, S. Min and F. Wang, Appl. Catal., B, 2019, 259,
- 229 C. Lai, Z. An, H. Yi, X. Huo, L. Qin, X. Liu, B. Li, M. Zhang, S. Liu, L. Li and others, J. Colloid Interface Sci., 2021, 600, 161-173.

- 230 J. Di, C. Chen, C. Zhu, P. Song, M. Duan, J. Xiong, R. Long, M. Xu, L. Kang, S. Guo and others, Nano Energy, 2021, 79, 105429.
- 231 S. Liu, W. Kuang, X. Meng, W. Qi, S. Adimi, H. Guo, X. Guo, E. Pervaiz, Y. Zhu, D. Xue and others, Chem. Eng. J., 2021, 416, 129116.
- 232 T. Rao, W. Cai, H. Zhang and W. Liao, J. Mater. Chem. C, 2021, 9, 5323-5342.
- 233 Z. Cheng, W. Qi, C. H. Pang, T. Thomas, T. Wu, S. Liu and M. Yang, Adv. Funct. Mater., 2021, 31, 2100553.
- 234 Y. Inoue, Energy Environ. Sci., 2009, 2, 364-386.
- 235 K. Maeda, K. Teramura, N. Saito, Y. Inoue, H. Kobayashi and K. Domen, Pure Appl. Chem., 2006, 78, 2267-2276.
- 236 L. Yuliati, J. H. Yang, X. Wang, K. Maeda, T. Takata, M. Antonietti and K. Domen, J. Mater. Chem., 2010, 20, 4295-4298.
- 237 Y. Moriya, T. Takata and K. Domen, Coord. Chem. Rev., 2013, 257, 1957-1969.
- 238 M. Ahmed and G. Xinxin, Inorg. Chem. Front., 2016, 3, 578-590.
- 239 M. G. Kibria and Z. Mi, J. Mater. Chem. A, 2016, 4, 2801-2820.
- 240 Y. Jiang, P. Liu, Y. Chen, Z. Zhou, H. Yang, Y. Hong, F. Li, L. Ni, Y. Yan and D. H. Gregory, Appl. Surf. Sci., 2017, 391, 392-403.
- 241 A. Kumar, P. R. Thakur, G. Sharma, M. Naushad, A. Rana, G. T. Mola and F. J. Stadler, Environ. Chem. Lett., 2019, 17, 655-682.
- 242 X. Meng, W. Qi, W. Kuang, S. Adimi, H. Guo, T. Thomas, S. Liu, Z. Wang and M. Yang, J. Mater. Chem. A, 2020, 8, 15774-15781.
- 243 H. S. Jung, Y. J. Hong, Y. Li, J. Cho, Y. J. Kim and G. C. Yi, ACS Nano, 2008, 2, 637-642.
- 244 D. Wang, A. Pierre, M. G. Kibria, K. Cui, X. Han, K. H. Bevan, H. Guo, S. Paradis, A. R. Hakima and Z. Mi, Nano Lett., 2011, 11, 2353-2357.
- 245 Z. Zhang, Q. Qian, B. Li and K. J. Chen, ACS Appl. Mater. Interfaces, 2018, 10, 17419-17426.
- 246 Z. Li, L. Zhang, Y. Liu, C. Shao, Y. Gao, F. Fan, J. Wang, J. Li, J. Yan, R. Li and others, Angew. Chem., 2020, 132, 945-952.
- 247 J. Winnerl, M. Kraut, S. Artmeier and M. Stutzmann, Nanoscale, 2019, 11, 4578-4584.
- 248 J. Li, W. Yang, A. Wu, X. Zhang, T. Xu and B. Liu, ACS Appl. Mater. Interfaces, 2020, 12, 8583-8591.
- 249 M. Idrees, C. V. Nguyen, H. D. Bui, I. Ahmad and B. Amin, Phys. Chem. Chem. Phys., 2020, 22, 20704-20711.
- 250 R. Li, W. H. Cheng, M. H. Richter, J. S. Du Chene, W. Tian, C. Li and H. A. Atwater, ACS Energy Lett., 2021, 6, 1849–1856.
- 251 L. Zhou, H. Zhang, H. Sun, S. Liu, M. O. Tade, S. Wang and W. Jin, Catal. Sci. Technol., 2016, 6, 7002-7023.
- 252 G. Liao, Y. Gong, L. Zhang, H. Gao, G.-J. Yang and B. Fang, Energy Environ. Sci., 2019, 12, 2080-2147.
- 253 S. K. Verma, R. Verma, Y. R. Girish, F. Xue, L. Yan, S. Verma, M. Singh, Y. Vaishnav, A. B. Shaik, R. R. Bhandare and others, Green Chem., 2022, 24, 438-479.

- 254 M. Zhang, Y. Yang, X. An and L. Hou, Chem. Eng. J., 2021, 412, 128663.
- 255 A. Mishra, A. Mehta, S. Basu, N. P. Shetti, K. R. Reddy and T. M. Aminabhavi, Carbon, 2019, 149, 693-721.
- 256 S. Patnaik, D. P. Sahoo and K. Parida, Carbon, 2021, 172, 682-711.
- 257 H. S. Gujral, G. Singh, A. V. Baskar, X. Guan, X. Geng, A. V. Kotkondawar, S. Rayalu, P. Kumar, A. Karakoti and A. Vinu, Sci. Technol. Adv. Mater., 2022, 23, 76-119.
- 258 X. Wang, K. Maeda, A. Thomas, K. Takanabe, G. Xin, J. M. Carlsson, K. Domen and M. Antonietti, Nat. Mater., 2009, 8, 76-80.
- 259 S. H. Li, M. Y. Qi, Z. R. Tang and Y. J. Xu, Chem. Soc. Rev., 2021, 50, 7539-7586.
- 260 J. F. Callejas, J. M. McEnaney, C. G. Read, J. C. Crompton, A. J. Biacchi, E. J. Popczun, T. R. Gordon, N. S. Lewis and R. E. Schaak, ACS Nano, 2014, 8, 11101-11107.
- 261 Y. Ni, L. Jin and J. Hong, Nanoscale, 2011, 3, 196-200.
- 262 S. Li, L. Wang, N. Xiao, A. Wang, X. Li, Y. Gao, N. Li, W. Song, L. Ge and J. Liu, Chem. Eng. J., 2019, 378, 122220.
- 263 Y. Song, X. Xin, S. Guo, Y. Zhang, L. Yang, B. Wang and X. Li, Chem. Eng. J., 2020, 384, 123337.
- 264 S. Cao, Y. Chen, C. J. Wang, X. J. Lv and W. F. Fu, Chem. Commun., 2015, 51, 8708-8711.
- 265 S. Cao, C. J. Wang, W. F. Fu and Y. Chen, ChemSusChem, 2017, 10, 4306-4323.
- 266 Y. Han, Y. Chen, R. Fan, Z. Li and Z. Zou, *EcoMat*, 2021, 3, e12097.
- 267 Z. Hu, Z. Shen and C. Y. Jimmy, Green Chem., 2017, 19, 588-613.
- 268 X. Yue, S. Yi, R. Wang, Z. Zhang and S. Qiu, Small, 2017, 13, 1603301.
- 269 P. Wang, S. Zhan, H. Wang, Y. Xia, Q. Hou, Q. Zhou, Y. Li and R. R. Kumar, Appl. Catal., B, 2018, 230, 210-219.
- 270 J. Wang, J. Chen, P. Wang, J. Hou, C. Wang and Y. Ao, Appl. Catal., B, 2018, 239, 578-585.
- 271 Z. Sun, M. Zhu, X. Lv, Y. Liu, C. Shi, Y. Dai, A. Wang and T. Majima, Appl. Catal., B, 2019, 246, 330-336.
- 272 L. Hong, R. Guo, Y. Yuan, X. Ji, Z. Lin, Z. Li and W. Pan, ChemSusChem, 2021, 14, 539-557.
- 273 H. Zhou, R. Chen, C. Han, P. Wang, Z. Tong, B. Tan, Y. Huang and Z. Liu, J. Colloid Interface Sci., 2022, 610, 126-135.
- 274 R. Liang, Y. Wang, C. Qin, X. Chen, Z. Ye and L. Zhu, Langmuir, 2021, 37, 3321-3330.
- 275 G. Fan, F. Li, D. G. Evans and X. Duan, Chem. Soc. Rev., 2014, 43, 7040-7066.
- 276 H. Boumeriame, E. S. Da Silva, A. S. Cherevan, T. Chafik, J. L. Faria and D. Eder, J. Energy Chem., 2022, 64,
- 277 Y. Zhao, X. Jia, G. I. N. Waterhouse, L. Z. Wu, C. H. Tung, D. O'Hare and T. Zhang, Adv. Energy Mater., 2016, 6, 1501974.
- 278 L. Mohapatra and K. Parida, J. Mater. Chem. A, 2016, 4, 10744-10766.

- 279 M. J. Wu, J. Z. Wu, J. Zhang, H. Chen, J. Z. Zhou, G. R. Qian, Z. P. Xu, Z. Du and Q. L. Rao, Catal. Sci. Technol., 2018, 8, 1207-1228.
- 280 C. Prasad, H. Tang, Q. Q. Liu, S. Zulfigar, S. Shah and I. Bahadur, J. Mol. Liq., 2019, 289, 111114.
- 281 G. Arrabito, A. Bonasera, G. Prestopino, A. Orsini, A. Mattoccia, E. Martinelli, B. Pignataro and P. G. Medaglia, Crystals, 2019, 9, 361.
- 282 A. Sherryna, M. Tahir and W. Nabgan, Int. J. Hydrogen Energy, 2021, 47, 862-901.
- 283 A. Razzaq, S. Ali, M. Asif and S. I. In, Catalysts, 2020, 10,
- 284 M. P. Jerome, F. A. Abdulkarim, M. T. Salem and M. Tahir, I. Environ. Chem. Eng., 2022, 108151.
- 285 Z. Yang, F. Wang, C. Zhang, G. Zeng, X. Tan, Z. Yu, Y. Zhong, H. Wang and F. Cui, RSC Adv., 2016, 6, 79415-79436.
- 286 T. Cheng, H. Gao, G. Liu, Z. Pu, S. Wang, Z. Yi, X. Wu and H. Yang, Colloids Surf., A, 2022, 633, 127918.
- 287 Y. Wu, X. Li, H. Zhao, F. Yao, J. Cao, Z. Chen, D. Wang and Q. Yang, Chem. Eng. J., 2021, 426, 131255.
- 288 S. He, C. Yan, X. Z. Chen, Z. Wang, T. Ouyang, M. L. Guo and Z. Q. Liu, Appl. Catal., B, 2020, 276, 119138.
- 289 S. Guo, L. Yang, Y. Zhang, Z. Huang, X. Ren, E. I. Wei and X. Li, J. Alloys Compd., 2018, 749, 473-480.
- 290 A. Balapure, Y. Nikhariya, N. S. Sriteja Boppudi, R. Ganesan and J. Ray Dutta, ACS Appl. Mater. Interfaces, 2020, 12, 21481-21493.
- 291 A. Balapure, H. Mude, P. Tata, J. R. Dutta and R. Ganesan, J. Environ. Chem. Eng., 2021, 9, 106065.
- 292 B. Li, Z. Cao, S. Wang, Q. Wei and Z. Shen, Dalton Trans., 2018, 47, 10288-10298.
- 293 Q. Chen, M. Zhang, J. Li, G. Zhang, Y. Xin and C. Chai, Chem. Eng. J., 2020, 389, 124476.
- 294 B. Wang, C. Chen, Y. Jiang, P. Ni, C. Zhang, Y. Yang, Y. Lu and P. Liu, Chem. Eng. J., 2021, 412, 128690.
- 295 L. Wang, G. Tang, S. Liu, H. Dong, Q. Liu, J. Sun and H. Tang, Chem. Eng. J., 2022, 428, 131338.
- 296 A. Bahadoran, S. Ramakrishna, S. Masudy-Panah, J. R. De Lile, J. Gu, Q. Liu and Y. K. Mishra, Ind. Eng. Chem. Res., 2022, 61, 10931-10944.
- 297 Z. Guan, Z. Xu, Q. Li, P. Wang, G. Li and J. Yang, Appl. Catal., B, 2018, 227, 512-518.
- 298 M. Zhang, C. Lai, B. Li, F. Xu, D. Huang, S. Liu, L. Qin, Y. Fu, X. Liu and H. Yi, Chem. Eng. J., 2020, 396, 125343.
- 299 X. Liu, C. Bie, B. He, B. Zhu, L. Zhang and B. Cheng, Appl. Surf. Sci., 2021, 554, 149622.
- 300 Y. Jiang, Z. Sun, Q. Chen, C. Cao, Y. Zhao, W. Yang, L. Zeng and L. Huang, Appl. Surf. Sci., 2022, 571, 151287.
- 301 D. Kong, X. Ruan, J. Geng, Y. Zhao, D. Zhang, X. Pu, S. Yao and C. Su, Int. J. Hydrogen Energy, 2021, 46, 28043-28052.
- 302 L. Zhu, H. Li, Z. Liu, P. Xia, Y. Xie and D. Xiong, J. Phys. Chem. C, 2018, 122, 9531-9539.
- 303 Y. Sun, X. Wang, Q. Fu and C. Pan, Appl. Surf. Sci., 2021, 564, 150379.

- 304 C. Hao, Y. Tang, W. Shi, F. Chen and F. Guo, Chem. Eng. J., 2021, 409, 128168.
- 305 B. Tahir and M. Tahir, Appl. Surf. Sci., 2020, 506, 145034.
- 306 Z. Kong, J. Zhang, H. Wang, B. Cui, J. Zeng, X. Chen, P. Tian, G. Huang, J. Xi and Z. Ji, Int. J. Energy Res., 2020, 44, 1205-1217.
- 307 H. Hou and X. Zhang, Chem. Eng. J., 2020, 395, 125030.
- 308 R. Xiao, C. Zhao, Z. Zou, Z. Chen, L. Tian, H. Xu, H. Tang, Q. Liu, Z. Lin and X. Yang, Appl. Catal., B, 2020, 268, 118382.
- 309 Q. Wang, H. Zhu and B. Li, Chem. Eng. J., 2019, 378, 122072.
- 310 M. Wang, M. Shen, L. Zhang, J. Tian, X. Jin, Y. Zhou and J. Shi, Carbon, 2017, 120, 23-31.
- 311 M. Z. Qin, W. X. Fu, H. Guo, C. G. Niu, D. W. Huang, C. Liang, Y. Y. Yang, H. Y. Liu, N. Tang and Q. Q. Fan, Adv. Colloid Interface Sci., 2021, 297, 102540.

- 312 B. Zhu, B. Cheng, J. Fan, W. Ho and J. Yu, Small Struct., 2021, 2, 2100086.
- 313 Q. Zhu, Y. Sun, S. Xu, Y. Li, X. Lin and Y. Qin, J. Hazard. Mater., 2020, 382, 121098.
- 314 A. Balapure, M. M. Francis, H. Mude, P. A. Maroju, J. R. Dutta and R. Ganesan, Carbon Trends, 2021, 5, 100118.
- 315 A. Balapure and R. Ganesan, J. Colloid Interface Sci., 2021, 581, 205-217.
- 316 M. M. Francis, A. Thakur, A. Balapure, J. R. Dutta and R. Ganesan, Chem. Eng. J., 2022, 446, 137363.
- 317 S. Li, H. Shang, Y. Tao, P. Li, H. Pan, Q. Wang, S. Zhang, H. Jia, H. Zhang, J. Cao, B. Zhang, R. Zhang, G. Li, Y. Zhang, D. Zhang and H. Li, Angew. Chem., Int. Ed., 2023, 62, e202305538.
- 318 Y. Tao, Z. Ma, W. Wang, C. Zhang, L. Fu, Q. Zhu, Y. Li, G. Li and D. Zhang, Adv. Funct. Mater., 2023, 33, 2211169.
- 319 A. Akhundi, A. Badiei, G. M. Ziarani, A. Habibi Yangjeh, M. J. Munoz-Batista and R. Luque, Mol. Catal., 2020, 488, 110902.